

## Research Article

# Glacial Lake Area Changes in High Mountain Asia during 1990–2020 Using Satellite Remote Sensing

Meimei Zhang,<sup>1,2</sup> Fang Chen ,<sup>1,2,3</sup> Huadong Guo,<sup>1,2,3</sup> Lu Yi,<sup>4</sup> Jiangyuan Zeng,<sup>5</sup> and Bin Li<sup>1,2</sup>

<sup>1</sup>International Research Center of Big Data for Sustainable Development Goals, Beijing 100094, China

<sup>2</sup>Key Laboratory of Digital Earth Science, Aerospace Information Research Institute, Chinese Academy of Sciences, No. 9 Dengzhuang South Road, Beijing 100094, China

<sup>3</sup>University of Chinese Academy of Sciences, Beijing 100049, China

<sup>4</sup>Key Laboratory of Coastal Environment and Resources Research of Zhejiang Province, School of Engineering, Westlake University, Hangzhou 310024, China

<sup>5</sup>State Key Laboratory of Remote Sensing Science, Aerospace Information Research Institute, Chinese Academy of Sciences, Beijing 100094, China

Correspondence should be addressed to Fang Chen; [chenfang\\_group@radi.ac.cn](mailto:chenfang_group@radi.ac.cn)

Received 4 May 2022; Accepted 13 September 2022; Published 27 October 2022

Copyright © 2022 Meimei Zhang et al. Exclusive Licensee Science and Technology Review Publishing House. Distributed under a Creative Commons Attribution License (CC BY 4.0).

Changes in a large-scale glacial lake area directly reflect the regional glacier status and climate changes. However, long time series of glacial lake dataset and comprehensive investigation of the spatiotemporal changes in the glacial lake area in the whole High Mountain Asia (HMA) region remained elusive. Satellite remote sensing provides an indispensable way for dynamic monitoring of glacial lakes over large regions. But glacial lakes are quite small and discretely distributed, and the extraction of glacial lakes is usually influenced by clouds, snow/ice cover, and terrain shadows; thus, there is a lack of an automatic method to continuously monitor the dynamic changes of glacial lakes in a large scale. In this paper, we developed a per-pixel composited method named the “multitemporal mean NDWI composite” to automatically extract the glacial lake area in HMA from 1990 to 2020 using time-series Landsat data. There were 19,294 glacial lakes covering a total area of  $1471.85 \pm 366.42 \text{ km}^2$  in 1990, and 22,646 glacial lakes with an area of  $1729.08 \pm 461.31 \text{ km}^2$  in 2020. It is noted that the glacial lake area in the whole HMA region expanded by  $0.58 \pm 0.21\%/a$  over the past three decades, with high spatiotemporal heterogeneity. The glacial lake area increased at a consistent speed over time. The fastest expansion was in East Kun Lun at an average rate of  $2.01 \pm 0.54\%/a$ , while in the Pamir and Hengduan Shan, they show slow increases with rates of  $0.33 \pm 0.08\%/a$  and  $0.39 \pm 0.01\%/a$ , respectively, during 1990–2020. The greatest increase in lake area occurred at 5000–5200 m a.s.l., which increased by about  $45 \text{ km}^2$  (~25%). We conclude that the temperature rise and glacier thinning are the leading factors of glacial lake expansion in HMA, and precipitation is the main source of lake water increase in West Kun Lun. Using the proposed method, a large amount of Landsat images from successive years of melting seasons can be fully utilized to obtain a pixel-level composited cloud-free and solid snow/ice-free glacial lake map. The uncertainties from supraglacial ponds and glacial meltwater were also estimated to improve the reliability and comparability of glacial lake area changes among different regions. This study provides important technical and data support for regional climate changes, glacier hydrology, and disaster analysis.

## 1. Introduction

Glacial lakes are the joint product of global warming and glacier melting. Glacial lake changes are closely associated with climate changes and glacier activities and impact the local hydrologic cycles [1, 2]. High Mountain Asia (HMA) develops the most extensive glaciers in the middle and low latitudes [3, 4]. In addition to evaporation and flowing into

rivers, a fair amount of glacial meltwater is retained in the glacial lakes. This to some extent delays the loss of regional glacial water resources due to climatic warming [5, 6] but also directly leads to an increased risk and number of potentially dangerous glacial lakes [7]. HMA is known as the world’s Glacial Lake Outburst Flood (GLOF) vulnerability hotspot [1, 8], and its GLOF risk could nearly triple with the future rapid development of lakes [9]. In the periods of

1990 and 2018, it was estimated that the HMA glacial lakes experienced widespread areal expansion at an average rate of 15.2% [10], with large variability between different subregions and elevation ranges.

Glacial lake area extraction is basically important for two reasons. First, glacial lake coverage areas offer the basic data to determine the detailed lake outlines. Several recently released HMA glacial lake inventories [10, 11], which are mainly delineated manually from Landsat images for the boundaries, can be used to provide the fundamental data for glacial lake change detection, GLOF hazard analysis, and terrestrial water budgets. Second, glacial lake coverage and associated area changes are closely related to glacier mass balance changes and regional climate conditions. Simulation results showed that more than 13,000 new glacial lakes could appear in the nonglacial area, and ~47% of them will appear by 2050 [9]. However, for all HMA glacial lakes, there are few long-term, continuous, and systematic observations of area changes so far. Most of the efforts are concerned with glacial lake monitoring over different regions of HMA at different time scales [12–14]. The resulting incomplete spatial coverage and the influence of different data sources and mapping algorithms yield large uncertainties in the regional comparisons and comprehensive evaluation of HMA [6, 15].

In the past decades, many studies have been carried out to delineate glacial lakes using optical remote sensing images. Manual digitalization through visual interpretation is still a necessary step for optimizing the mapping results. Water indices (WIs) [16–18] combine two or more spectral bands by mathematical computation and are effective and convenient for water detection. The combination of WI maps with several segmentation methods, such as iterative threshold segmentations [19–21] and level-set-based active-contour approaches [15, 22], has been proposed to improve the lake local details. Nevertheless, a number of manual postprocessing steps were required to remove other false water features (e.g., small streams and shadows) and supplement missing lakes. Object-oriented analysis of remote sensing data that included size, shape, reflectance, and contextual information was performed for mapping glacial lakes with specific morphological and spectral features [21, 23]. Machine learning, such as random forest and deep learning methods, has high generalization and automation ability for recognizing glacial lakes from high-dimensional data, while the results heavily rely on the appropriate training samples. Additionally, the requirements for both costs and processing times are exceptionally high [24–26]. Despite the achieved inspiring results, for HMA, the extraction of small and dispersed glacial lake targets over such a large-scale area with harsh climate and complex terrain conditions is challenging. Among the aforementioned methods, WIs are the most popular method for glacial lake extraction due to their high computational efficiency and ease of use, and among different WIs, the normalized difference water index (NDWI) [16] is robust in delineating different types of lakes and features a reasonably stable threshold to classify edge pixels of water [18, 27].

Glacial lakes are defined as water bodies originating from glacier activities, which are formed when glaciers erode the

lands and melt and fill depressions excavated by glaciers [28]. According to the definition of glacial lakes, they are distributed around glaciers, and a 10 km buffer [11, 29] around the Randolph Glacier Inventory (RGI v6.0) [30] was widely used to preliminarily determine the distribution area of glacial lakes. Within this 10 km buffer range, some researchers only define the lakes that are directly fed by glaciers as glacial lakes [31, 32], but others think that all the lakes within the buffer are glacial lakes and can be further divided into different subclasses according to whether they are supplied by glaciers and whether they are connected with glaciers [10, 33]. There are no unified classification schemes for glacial lakes. Unlike glaciers that appear as perennial, large pieces of dense ice slowly moving under their own weight, glacial lakes are abundant at small size and have high spatial variability. Due to the changeable environment and the complex spectral features of satellite images, the great challenges of automatically detecting glacial lakes from optical data include the following obstacles: identifying clouds and alleviating their impacts, excluding mountain shadows, distinguishing glacial lakes from snow and ice cover, and detecting the changing pattern of glacial lakes.

Summer and autumn seasons are generally selected as the optimal time to recognize glacial lakes from satellite imagery because ice and seasonal snow melt and lakes present a stable extent during this period [34]. For the whole HMA, the situation is much more complicated. There is frequent solid precipitation in summer in the Himalayan regions [35], and this is especially pronounced on Tien Shan Mountain, where the precipitation is solid for the whole year at an elevation higher than 3000 m [36, 37]. The existence of clouds and seasonal snow cover in the warm season makes lake delineation challenging. Glacial lake inventory compilation for the southeastern Tibetan Plateau is extremely difficult due to the prevalent heavy clouds influenced by summer monsoons and high-relief terrain [38]. Although clouds and cloud shadows can be automatically detected from multispectral data and using time series of satellite scenes could reduce the impact of clouds, it is not possible to merge them together piecewise for large cloud-free optical imagery.

In rugged terrain environments, glacial lakes are easily confused with mountain shadows due to their similar spectral reflectance. This phenomenon is particularly serious for north-facing glaciers that are widely shaded by adjacent mountains [39]. Slope maps and shaded relief derived from a digital elevation model (DEM) have been employed to mask a number of mountain shadows [9, 22]. To completely eliminate the interference of mountain shadows, their spatial relationships with regard to glacial lakes should be modeled, which requires many additional parameters such as solar elevation angle, local time of image, and relative height difference between glacial lakes and mountain peaks [40]. It is not easy to identify mountain shadows in large regions.

At present, there is no systematic studies to investigate the current distribution and spatiotemporal heterogeneity of glacial lakes in the whole HMA. The historical to present glacial lake dataset covering HMA is crucial for assessing glacier-climate change interactions and GLOF risk at the regional scale. Local residents and management agencies

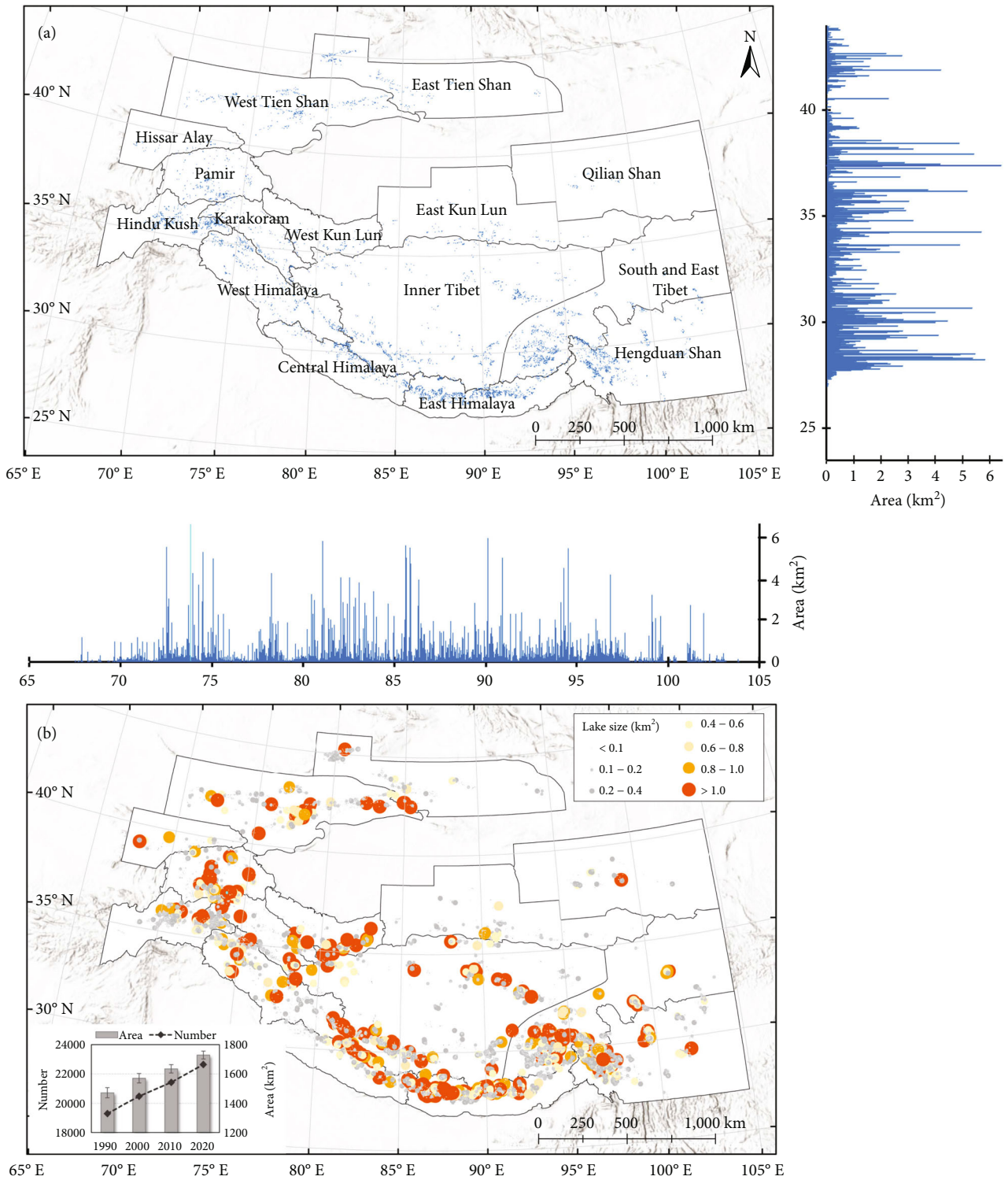


FIGURE 1: Glacial lake distribution in HMA in 2020. (a) The mapped glacial lake extent (blue polygons), and area statistics along latitude (right) and longitude (below); (b) distribution of different sizes of glacial lakes. The circle size represents the size class to which each glacial lake area belongs. The inset shows the total number and area of glacial lakes in 1990, 2000, 2010, and 2020.

are also very concerned about the development and changes of glacial lakes, in order to predict and give early warning of outburst disasters and minimize casualties and economic losses. Meanwhile, monitoring glacial lake changes in HMA as a whole is particularly important for assessing the

impacts of global climate changes. The spatial distribution and heterogeneous changes of rapidly expanding glacial lakes in the whole HMA region deserve further attentions.

Google Earth Engine (GEE) is the most advanced geographic information processing platform based on cloud

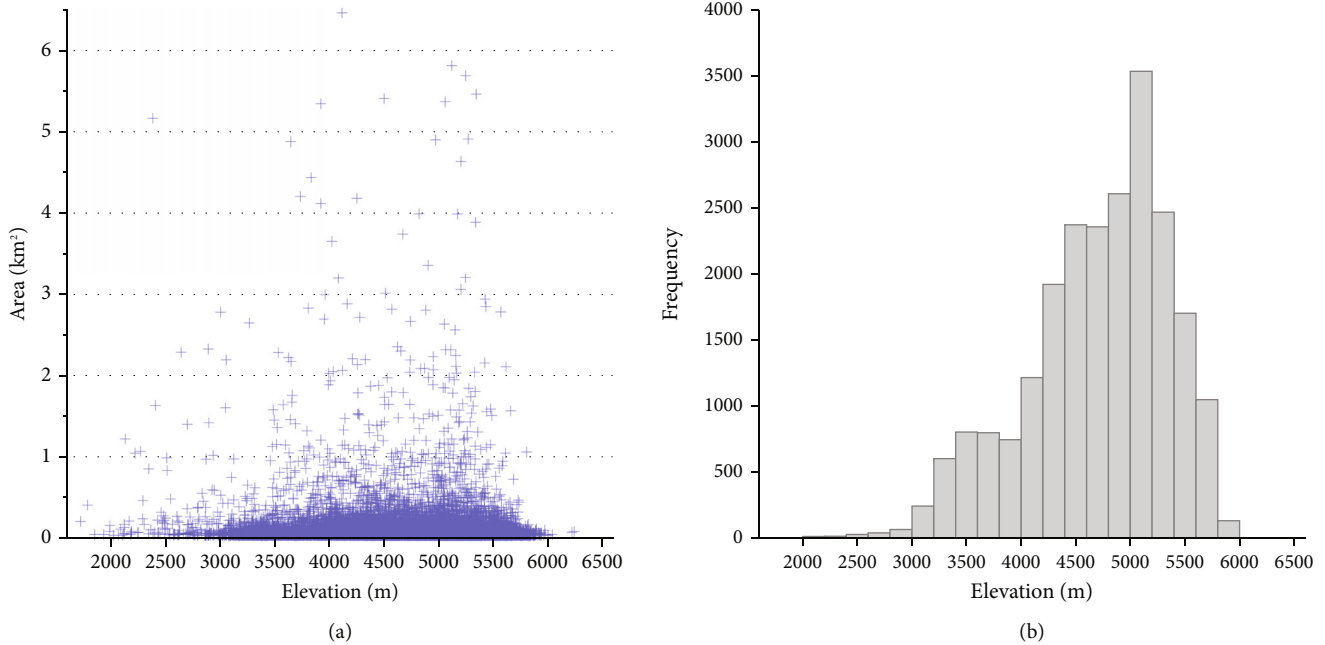


FIGURE 2: (a) Area distribution of glacial lakes along the elevation in 2020; (b) frequency distribution of glacial lakes along the elevation.

computing in the world. It offers the possibility for the large-scale processing and analysis of geoscience data and has become popular in land-cover classification [41–43]. For mapping glacial lakes over the whole HMA region, a reasonable and effective strategy is still lacking. In the study of the extraction of glacial lake outlines using this cloud-based platform, the scheme of glacial lake mapping in the Third Pole is discussed [22]. However, the GEE is mainly used for the selection of cloudless images, and we noted the post-processing problems regarding manual reediting and removing some erroneously extracted lakes in their semiautomated method. Therefore, in this study, we developed a new automatic method—the multitemporal mean NDWI composite—to extract glacial lakes based on the archived Landsat data on GEE. Then, the glacial lake coverage over the whole HMA was extracted with the proposed method, and long-term changes in the glacial lake area from 1990 to 2020 were estimated in detail.

## 2. Results

**2.1. Spatial Distribution Pattern of Glacial Lakes.** Based on the developed glacial lake mapping method, the glacial lake areas across the 15 subregions in HMA were extracted at 10-year intervals from 1990 to 2020. An example of the latest distribution pattern of glacial lakes in 2020 is presented in Figure 1. Most of the glacial lakes were developed in the southern zone of HMA, including Hindu Kush-Karakoram-Himalaya Mountain ranges, South and East Tibet, and Hengduan Shan (Figure 1(a)), where large glacial lakes ( $>1 \text{ km}^2$ ) were also distributed over these regions (Figure 1(b)). In East Kun Lun and Qilian Shan, glacial lakes were sparsely distributed, and almost all were in small sizes. Glacial lake area is evenly distributed along the longitude, but concentrated in the latitude range between  $27^\circ\text{N}$  and  $32^\circ\text{N}$  and also around  $35^\circ\text{N}$ , corresponding

to the Central and East Himalaya, the south side of South and East Tibet, and the Hengduan Shan (Figure 1(a)). In 2020, only 214 large glacial lakes ( $>1 \text{ km}^2$ ) were identified. Glacial lakes with an area of less than  $1 \text{ km}^2$  covered  $1337.36 \pm 261.47 \text{ km}^2$ , accounting for  $77.35 \pm 18.16\%$  of the total lake area ( $1729.08 \pm 461.31 \text{ km}^2$ ). 19,131 glacial lakes ( $578.37 \pm 121.45 \text{ km}^2$ ) are less than  $0.1 \text{ km}^2$ , which is dominated in number (84%). Compared with the very large glacial lakes, the spatial and temporal variation of these small lakes is significant due to the unstable shapes and enhanced hydrological cycle [21].

Figure 2 shows the distribution pattern of glacial lakes in the vertical direction in 2020. Glacial lakes were distributed between 2000 m a.s.l. and 6000 m a.s.l. Most of the glacial lakes were located at the elevation above 3500 m a.s.l., and the main elevation range of the glacial lake distribution was 4200–5500 m a.s.l. These results are consistent well with the previous studies [10, 11, 31]. In each 200 m bin size, more than 3500 glacial lakes were found in the 5000–5200 m a.s.l., which further confirm that as the global temperature rises, more glacial lakes gradually develop towards higher elevations [44].

**2.2. Area Changes in Glacial Lakes in HMA.** Due to the occurrence of snow or ice meltwater on the glacier terminus and the limited observation times of each pixel used for the image composite in some regions, the extracted glacial lake pixels cannot be directly used for the calculation and analysis of glacial lake area changes. To reduce the total bias in the estimated lake area and improve the reliability of results, lake area uncertainty is estimated by an error of areas corresponding to the lake region within the glacier boundaries. Our mapped glacial lake pixels corresponding to the region outside of glacier boundaries are used as the lower limit,



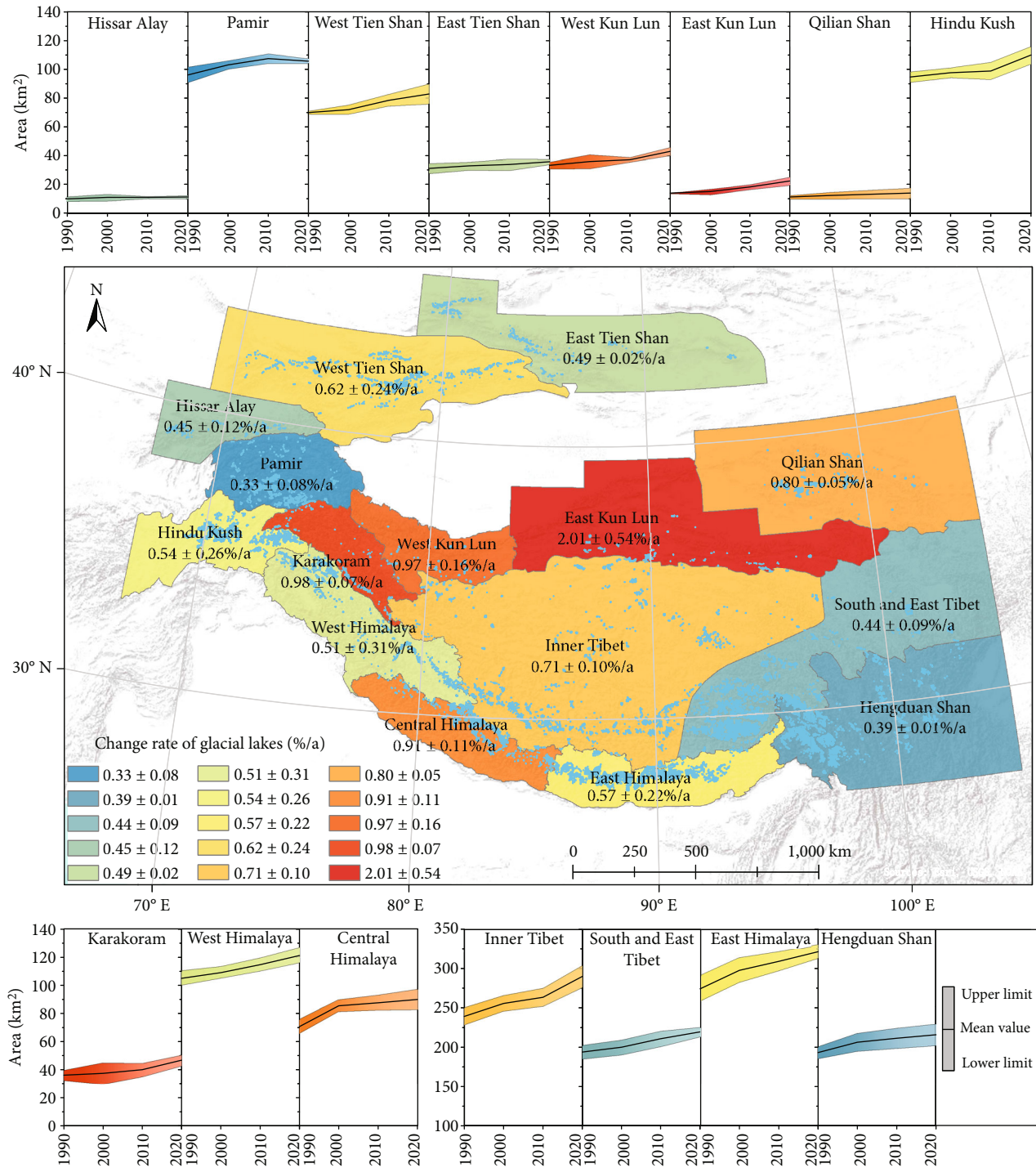


FIGURE 3: Glacial lake area changes in HMA during 1990–2020. Map in the center displays the spatial extent of HMA, glacial lake distribution (blue polygons) in 2020, and the average change rate in each subregion during 1990–2020. Banded curves in different colors denote the detailed glacial lake area changes in different periods and different subregions.

and all glacial lake pixels are deemed the upper limit. The areas within the upper and lower limits in different colors in Figure 3 denote the glacial lake area changes of each subregion during 1990–2020. Considering the presence of unstable supraglacial lakes on the glacier surface, the estimated glacial lake area of each subregion is obtained by averaging the upper and lower limits.

We do not adopt the uncertainty estimation methods used in the previous studies by the linear error and the lake’s perimeter [39, 45, 46]. The main reasons are as follows: (1) the proposed automated mapping method is based on the pixel-level composited, and the output glacial lake maps are in raster format displaying the glacial lake coverage areas, while others are vectorized glacial lake outlines; (2)

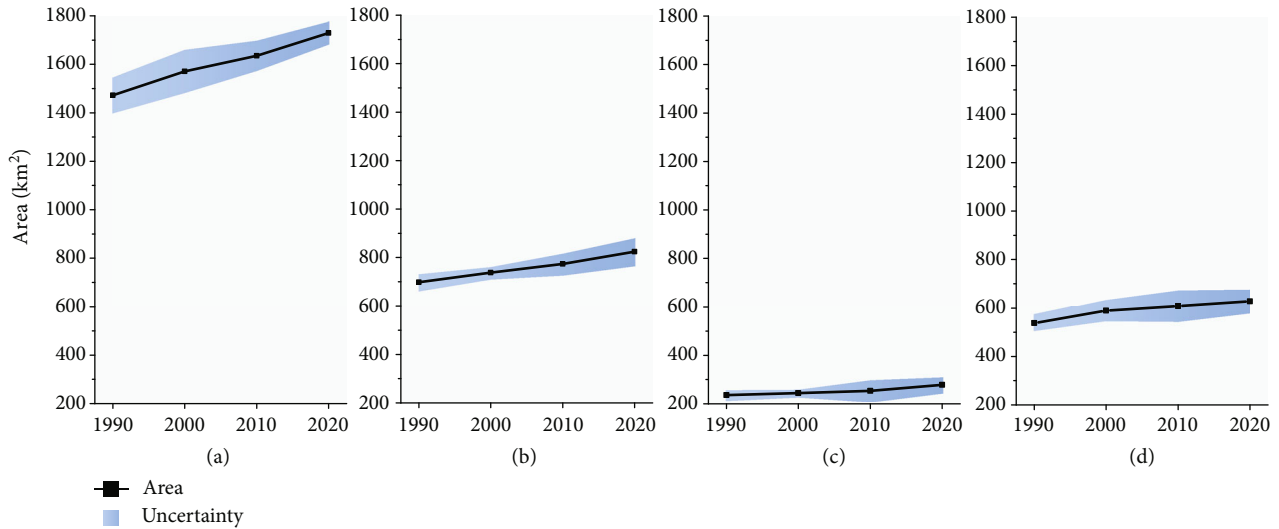


FIGURE 4: Glacial lake area changes from 1990 to 2020 for (a) the whole HMA, (b) Central Asia (including Hissar Alay, Pamir, West Tien Shan, East Tien Shan, West Kun Lun, East Kun Lun, Qilian Shan, Inner Tibet, and South and East Tibet), (c) South Asia West (including Hindu Kush, Karakoram, and West Himalaya), and (d) South Asia East (including Central Himalaya, East Himalaya, and Hengduan Shan).

the effects from supraglacial ponds and glacial meltwater and the limited observation times are fully considered in this study. Based on the calculated glacial lake areas and their uncertainty measurements, the area change rates between 1990 and 2020 in different regions are calculated.

The lake area change with time varies greatly among different regions across the HMA. All the 15 subregions showed varying degrees of expansion. This is expected due to the continued global warming (especially in the HMA region) over the past several decades [47, 48]. The most rapid expansion in the glacial lake area is in East Kun Lun at a rate of approximately  $2.01 \pm 0.54\%/a$ , but with a small total area ( $22.30 \pm 4.36 \text{ km}^2$  in 2020). There has been little expansion in Hengduan Shan during the past 30 years. In Pamir, the glacial lake areas increased rapidly during 1990–2010, but slightly decreased and became relatively stable in the following 10 years, resulting in the slowest expansion rate ( $0.33 \pm 0.08\%/a$ ). It should be noted that in West Kun Lun, where the glacier area was recorded to increase at a rate of  $0.50 \pm 0.11\%/a$  during 1990–2018 [49], glacial lakes in this region also unexpectedly exhibited an increasing area in recent years.

The changes in the glacial lake area in the whole HMA and Region 13 Central Asia, Region 14 South Asia West, and Region 15 South Asia East are shown in Figure 4. Glacial lakes expanded at rates of  $0.60 \pm 0.17\%/a$ ,  $0.59 \pm 0.23\%/a$ , and  $0.55 \pm 0.11\%/a$  between 1990 and 2020 for Central Asia, South Asia West, and South Asia East, respectively. The total glacial lake area in HMA expanded by  $257.23 \pm 94.89 \text{ km}^2$  ( $17.47 \pm 6.33\%$ ) at a rate of  $0.58 \pm 0.21\%/a$  during 1990–2020. Specifically, the expansion rates of glacial lake area were  $0.67 \pm 0.12\%/a$  from 1990 to 2000,  $0.40 \pm 0.05\%/a$  from 2000 to 2010, and  $0.57 \pm 0.09\%/a$  from 2010 to 2020, with a continuous and uniformly expanding trend in the past 30 years.

**2.3. Different Patterns of Glacial Lake Evolution.** In order to explore the dynamic evolution process of glacial lakes in more

detail, the annual area changes of glacial lakes aggregated on a grid of  $1^\circ \times 1^\circ$  were further analyzed (Figure 5(a)). Negative growth of glacial lake area was observed in East Hindu Kush, Karakoram, Inner Tibet, and Hengduan Shan. The region with the fastest area decrease was in the Karakoram Mountain, with a negative area rate of  $-0.44 \text{ km}^2/a$ , where a medium-sized glacial lake ( $0.4\text{--}0.6 \text{ km}^2$ ) had vanished during 1990–2020 (Figure 5(b)). In contrast, the areas of glacial lakes in most of the other mountains continue to expand. The fastest growing region ( $0.85 \text{ km}^2/a$ ) is located in the East Himalaya, with the emergence of many medium and large glacial lakes in 2020 (Figure 5(c)). It is noted that a new glacial lake with an area of larger than  $1 \text{ km}^2$  has appeared in the West Tien Shan, which also correspond with the rapidly expanding zone.

Both area and number of glacial lakes have increased at different 200 m elevation bands in HMA (Figure S1). The greatest expansion occurred at 5000–5200 m a.s.l., with the increased area of about  $45 \text{ km}^2$  ( $\sim 25\%$ ). The area change rate fluctuated at different elevation ranges with no obvious trend. The glacial lake area changes with elevation were significantly different among the different subregions (Figure 6). The change rates of glacial lakes in the West Tien Shan, East Tien Shan, Inner Tibet, and East Himalaya were found to be increasing with the increased elevation. However, the change rates varied markedly, and no significant trends of increase or decrease were observed in other subregions. In particular, glacial lakes in West Tien Shan and Karakoram exhibited large area decreases at elevations of about 3400 m a.s.l. ( $-1.99 \text{ km}^2$ ) and 4600 m a.s.l. ( $-2.60 \text{ km}^2$ ), respectively.

**2.4. Effects of Climate and Glacier Thickness Changes on the Glacial Lake Changes.** The heterogeneous changes in the glacial lake area in the whole HMA is closely related to complex climate changes and glacier activities. From 1990 to 2020, the temperature of all mountain ranges in HMA showed

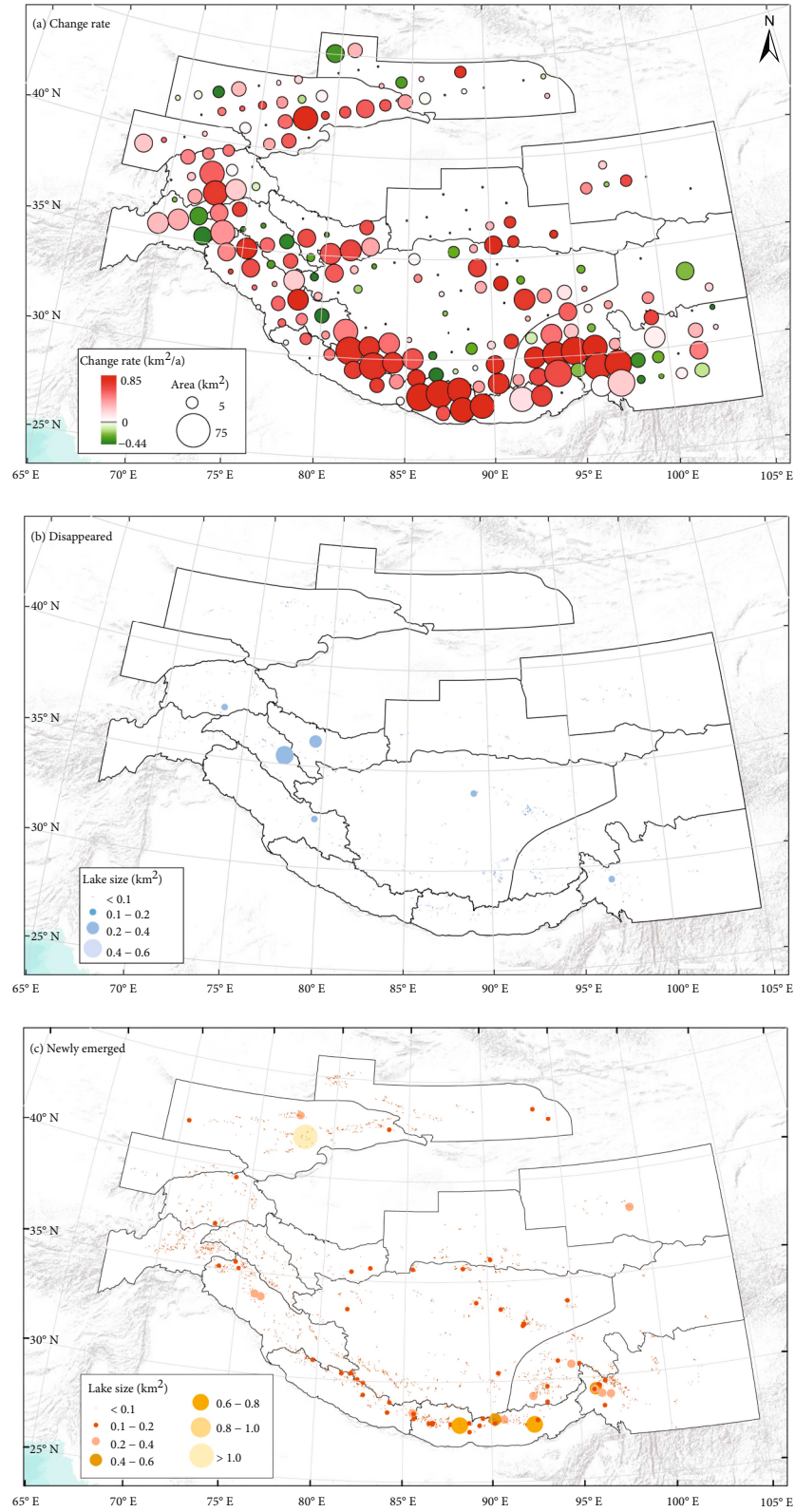


FIGURE 5: Evolution pattern of glacial lakes in HMA from 1990 to 2020. (a) Change rates in glacial lake area aggregated on a 1° × 1° grid. The circle size represents the total glacial lake area in 2020. (b) Disappeared glacial lakes. (c) Newly emerged glacial lakes.

an increasing trend, with the highest warming rate of 0.6°C/10a ( $P$  value < 0.05) occurring in Inner Tibet and West Tien Shan (Figure S2(a)).

Rapid increase in the glacial lake area in HMA appears to be directly driven by multiple water sources, including net precipitation falling into the lakes, surface runoff from

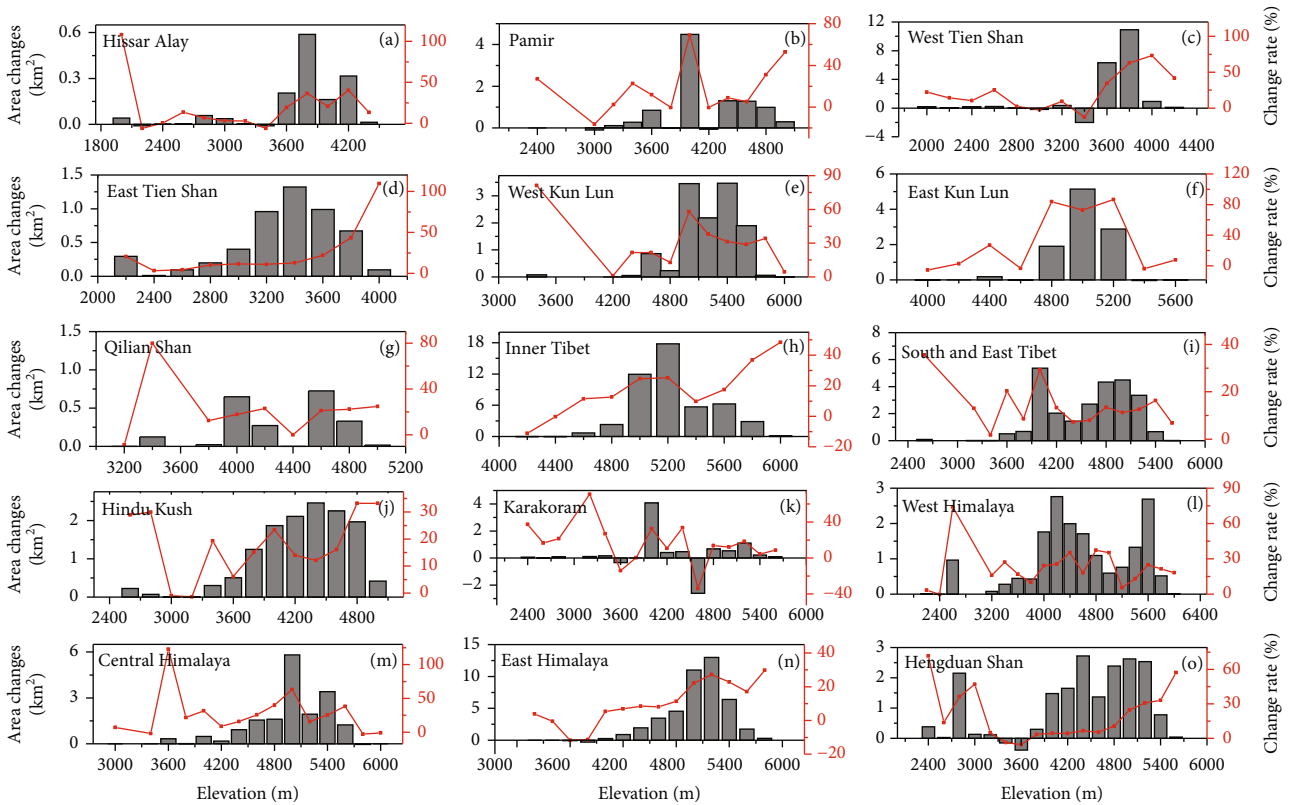


FIGURE 6: Changes in glacial lake area along the elevation (200 m bin sizes) for each subregion during 1990-2020.

precipitation, glacier melting, and permafrost degradation. Almost the entire Himalaya Mountain ranges, as well as parts of the West Tien Shan, Hindu-Kush, and Hengduan Shan, are getting drier, while Inner Tibet is getting wetter (Figure S2(b)). Many studies have reported that  $\sim 70\%$  of the increase in lake water in the endorheic basin (e.g., Inner Tibet) is due to the increased precipitation [50–52]. In the Himalayan region, precipitation decreased by up to 16 mm/a ( $P$  value  $< 0.05$ ), so the precipitation in these regions did not account for the main contribution of glacial lake expansion.

At the same time, the mountainous glacier activities caused by the climate changes are intensifying, such as the rapid retreat of glacier ablation area, glacier surface thinning, and glacier surge [4, 53, 54]. Glacier changes affect the development and expansion of glacial lakes from several aspects. Glacier surface thinning provides source of water for the glacial lake area expansion, while the rapid retreat of the glacier terminus provides sufficient space for the development of glacial lakes. In this paper, to illustrate the effects of regional glacier surface elevation changes on the glacial lake changes, West Tien Shan, West Kun Lun, and East Himalaya were selected as the typical mountain regions due to the observed great total mass loss across the Tien Shan and Himalaya and significant positive mass change in the West Kun Lun [55–57]. As each subregion is very huge, it is difficult to show the glacier surface elevation changes at glacier-specific scale clearly. Therefore, partial regions in the three mountains with the most representative glacier changes and densely distributed glacial lakes surrounded are taken as examples (Figure S3). From 2000 to 2018, the glacier surface

elevations in West Tien Shan and East Himalaya showed significant thinning, with the mean negative elevation changes of  $-0.24 \pm 0.07$  m/a and  $-0.39 \pm 0.15$  m/a, respectively, and the mean thinning rate of glaciers in East Himalaya was faster. During this period, the glacier surface elevation of West Kun Lun showed a thickening trend of  $0.23 \pm 0.10$  m/a due to the extensive glacier surge [56]. Overall, it can be inferred that the rapid expansion of glacial lakes in HMA since 1990 is mainly driven by climate warming and glacier thinning, and the local evolution patterns of glacial lakes are related to the regional differences of climate variability and glacier ablation. For some regions with abnormal glacier thickness changes such as West Kun Lun, increased precipitation dominates the spatial distribution and variation of glacial lakes.

**2.5. Evaluation of Extracted Glacial Lake Extent.** The extracted glacial lake areas in 1990 and 2020 were compared with the newly released glacial lake inventory in 1990 and 2018, which was produced by Wang et al. (2020) over a much larger region, including Altai and Sayan. To make the comparison in the same spatial extent and minimum mapping unit, we excluded the Altai and Sayan region and lakes smaller than  $0.0081$  km<sup>2</sup> from the inventory. The differences between the lake areas extracted in 1990 and 2020 and those derived from the inventory are illustrated in Figure 7.

Our mapped results show general agreement with the inventory data for most of the subregions having varying total lake areas. The most overestimated lake area is located in Central Himalaya, which is shown as an example in Figure 8 for



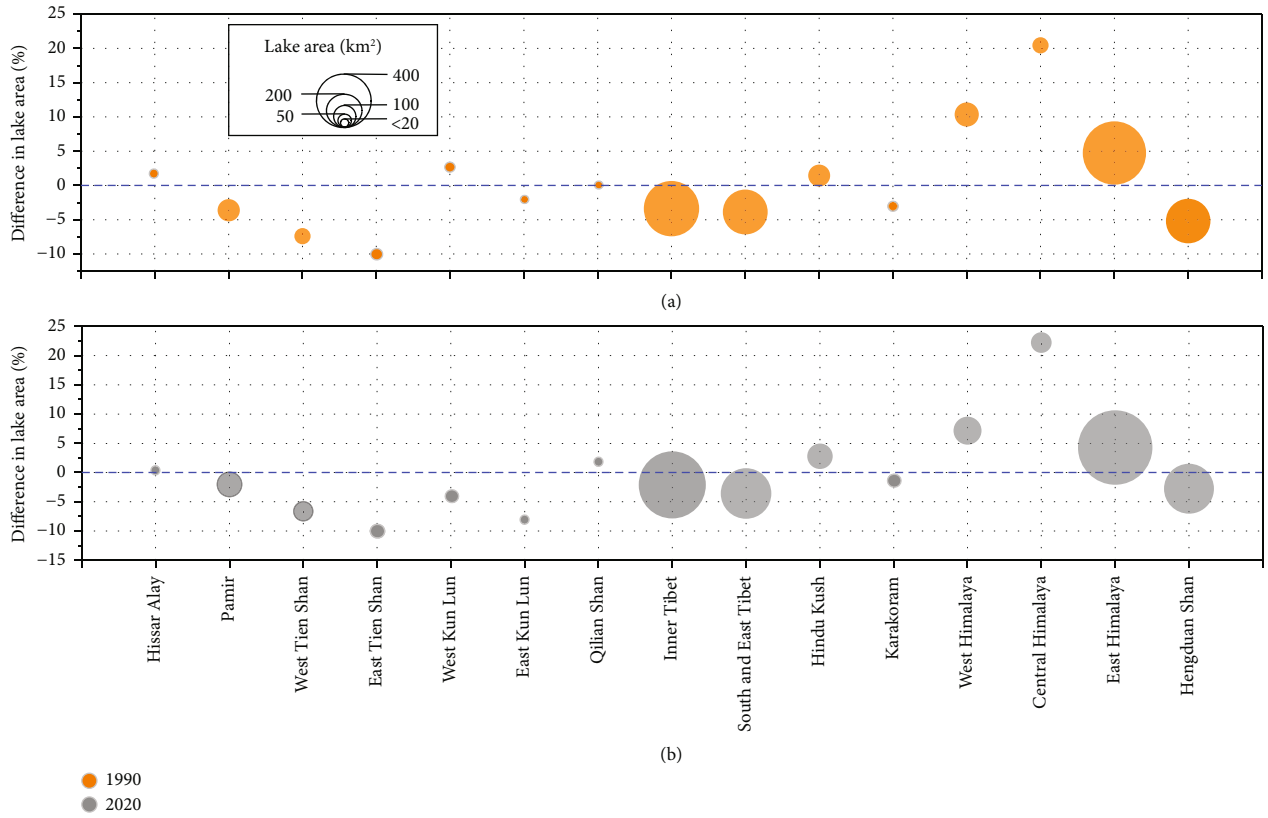


FIGURE 7: Differences in the extracted glacial lake areas in (a) 1990 and (b) 2020 with lake inventory from Wang et al. (2020). Bubble size denotes the total glacial lake area in each subregion.

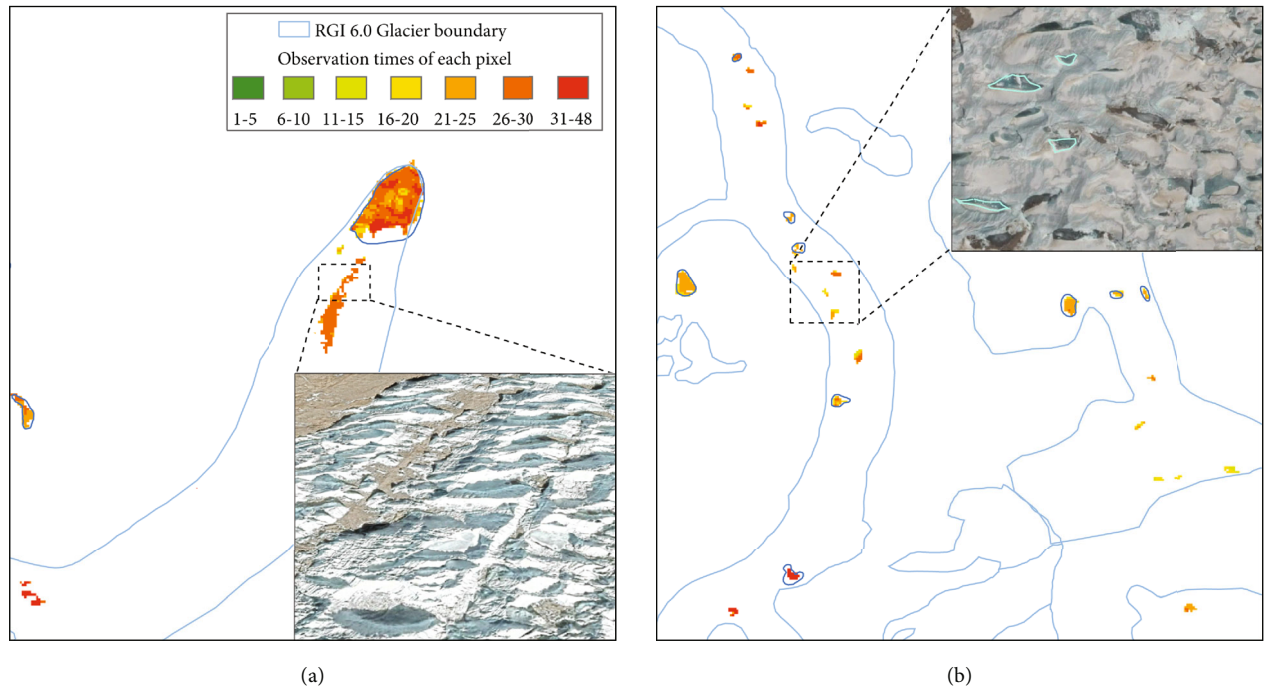


FIGURE 8: Examples showing the overestimated areas in Central Himalaya in 2020. (a) Snow and ice melt region on the glacier terminus; (b) supraglacial ponds formed on the debris-covered ablation zones. Dark blue polygons are the outlines from the glacial lake inventory. The two high-resolution Google Earth images are obtained on June 03, 2019, with supraglacial lakes shown in cyan outlines.

TABLE 1: Comparison of glacial lake area changes derived by our proposed method and previous studies. Statistics at different times in the columns of number and area are separated by slash. “c.” indicates that data are not recorded.

| Subregion            | This study    |             |           |                                   | References    |            |               |                               |                                 |        |
|----------------------|---------------|-------------|-----------|-----------------------------------|---------------|------------|---------------|-------------------------------|---------------------------------|--------|
|                      | Time interval | Rate (%/a)  | Number    | Area (km <sup>2</sup> )           | Time interval | Rate (%/a) | Number        | Area (km <sup>2</sup> )       | Study area                      | Source |
| Hissar Alay          | 1990–2020     | 0.45 ± 0.12 | 112/137   | 9.87 ± 1.97/11.20 ± 2.14          | 1990–2015     | 0.36       | 176/224       | 14.5 ± 0.2/15.8 ± 0.1         | The whole region                | [9]    |
| Pamir                | 1990–2010     | 0.58 ± 0.15 | 597/665   | 96.19 ± 18.44<br>/107.52 ± 23.65  | 1990–2013     | 0.45       | 238/188       | 78.01 ± 2.74<br>/86.07 ± 2.67 | West Tarim basin in the Pamir   | [59]   |
| West Tien Shan       | 1990–2010     | 0.62 ± 0.24 | 954/1124  | 69.90 ± 18.52<br>/78.53 ± 21.65   | 1990–2010     | 0.58       | 990/1146      | 60.64 ± 8.68<br>/67.73 ± 9.84 | The whole region                | [45]   |
| East Tien Shan       | 1990–2010     | 0.42 ± 0.08 | 586/714   | 31.11 ± 7.55/33.76 ± 6.52         | 1972–2007     | 0.98       | 66/132        | 2.56 ± 0.14<br>/3.44 ± 0.18   | Two Landsat scenes              | [62]   |
| West Kun Lun         | 1990–2010     | 0.59 ± 0.30 | 131/143   | 33.17 ± 5.19/37.14 ± 6.29         | 1990–2010     | 1.51       | 371/521       | 22.08 ± 3.19<br>/28.79 ± 4.39 | The whole region                | [45]   |
| East Kun Lun         | 1990–2020     | 2.01 ± 0.54 | 309/391   | 13.90 ± 3.38/22.30 ± 4.36         | 1990–2013     | 1.21       | 217/179       | 6.98 ± 1.10<br>/8.92 ± 1.19   | Tarim basin in the West Kun Lun | [59]   |
| Qilian Shan          | 1990–2020     | 0.80 ± 0.05 | 159/207   | 11.17 ± 2.65/13.86 ± 2.77         | 1990–2015     | 0.24       | 182/181       | 9.8 ± 0.2/10.4 ± 0.1          | The whole region                | [9]    |
| Inner Tibet          | 1990–2000     | 0.69 ± 0.22 | 3389/3552 | 239.05 ± 40.04<br>/255.65 ± 47.16 | 1990–2015     | 1.29       | 112/130       | 6.2 ± 0.1/8.2 ± 0.1           | The whole region                | [9]    |
| South and East Tibet | 1990–2010     | 0.44 ± 0.11 | 2762/2914 | 193.68 ± 35.96<br>/210.67 ± 37.95 | 1990–2000     | 0.86       | 275/300       | 28.9 ± 4.6/31.4 ± 5.0         | Inner Plateau basin             | [31]   |
| Hindu Kush           | 2000–2010     | 0.12 ± 0.04 | 1842/1853 | 97.68 ± 19.81<br>/98.91 ± 17.22   | 1988–2013     | 0.38       | 1278/<br>1396 | 85.24/93.31                   | One Landsat scene               | [60]   |
| Karakoram            | 1990–2000     | 0.36 ± 0.08 | 534/596   | 36.06 ± 7.33/37.38 ± 7.48         | 2001–2013     | -0.11      | -722          | 51.4/50.7                     | Hindu Kush in Pakistan          | [63]   |
|                      | 2000–2010     | 0.67 ± 0.17 | 596/629   | 37.38 ± 7.48/39.90 ± 9.15         | 1990–2000     | -3.6       | —             | —                             | One Landsat scene               | [14]   |
|                      | 1990–2010     | 0.53 ± 0.16 | 534/629   | 36.06 ± 7.33/39.90 ± 9.15         | 2000–2009     | 1.0        | -422          | -3.7                          | One Landsat scene               | [14]   |
| West Himalaya        | 1990–2020     | 0.51 ± 0.31 | 1525/1895 | 105.08 ± 20.35<br>/121.30 ± 24.67 | 2001–2013     | 1.64       | -1325         | 46.2/55.3                     | Karakoram in Pakistan           | [63]   |
| Central Himalaya     | 1990–2020     | 0.91 ± 0.11 | 1055/1304 | 70.68 ± 14.14<br>/89.92 ± 16.34   | 1990–2013     | 0.61       | 162/141       | 14.74 ± 1.13<br>/16.81 ± 1.09 | Tarim basin in the Karakoram    | [59]   |
| East Himalaya        | 1990–2020     | 0.57 ± 0.22 | 3189/3611 | 274.21 ± 44.95<br>/321.46 ± 54.29 | 1990–2015     | 0.22       | -979          | -50.0                         | North of ridge line             | [33]   |
| Hengduan Shan        | 1990–2010     | 0.47 ± 0.19 | 2279/2564 | 193.05 ± 35.75<br>/211.43 ± 38.44 | 1990–2015     | 0.20       | -476          | -38.8                         | South of ridge line             | [33]   |
|                      |               |             |           |                                   | 1990–2015     | 0.55       | -839          | -117.4                        | North of ridge line             | [33]   |
|                      |               |             |           |                                   | 1990–2015     | 0.92       | -1104         | -86.3                         | South of ridge line             | [33]   |
|                      |               |             |           |                                   | 1988–2015     | 2.00       | 107/148       | 4.62/7.12                     | Gyirong River basin             | [64]   |
|                      |               |             |           |                                   | 1990–2015     | 0.31       | -502          | -66.0                         | North of ridge line             | [33]   |
|                      |               |             |           |                                   | 1990–2015     | 0.44       | -1050         | -96.8                         | South of ridge line             | [33]   |
|                      |               |             |           |                                   | 1990–2014     | 0.12 ±     | 2872/         | 248.9 ± 29.9                  | The whole region                | [61]   |
|                      |               |             |           |                                   |               | 0.03       | 3235          | /255.8 ± 31.6                 |                                 |        |

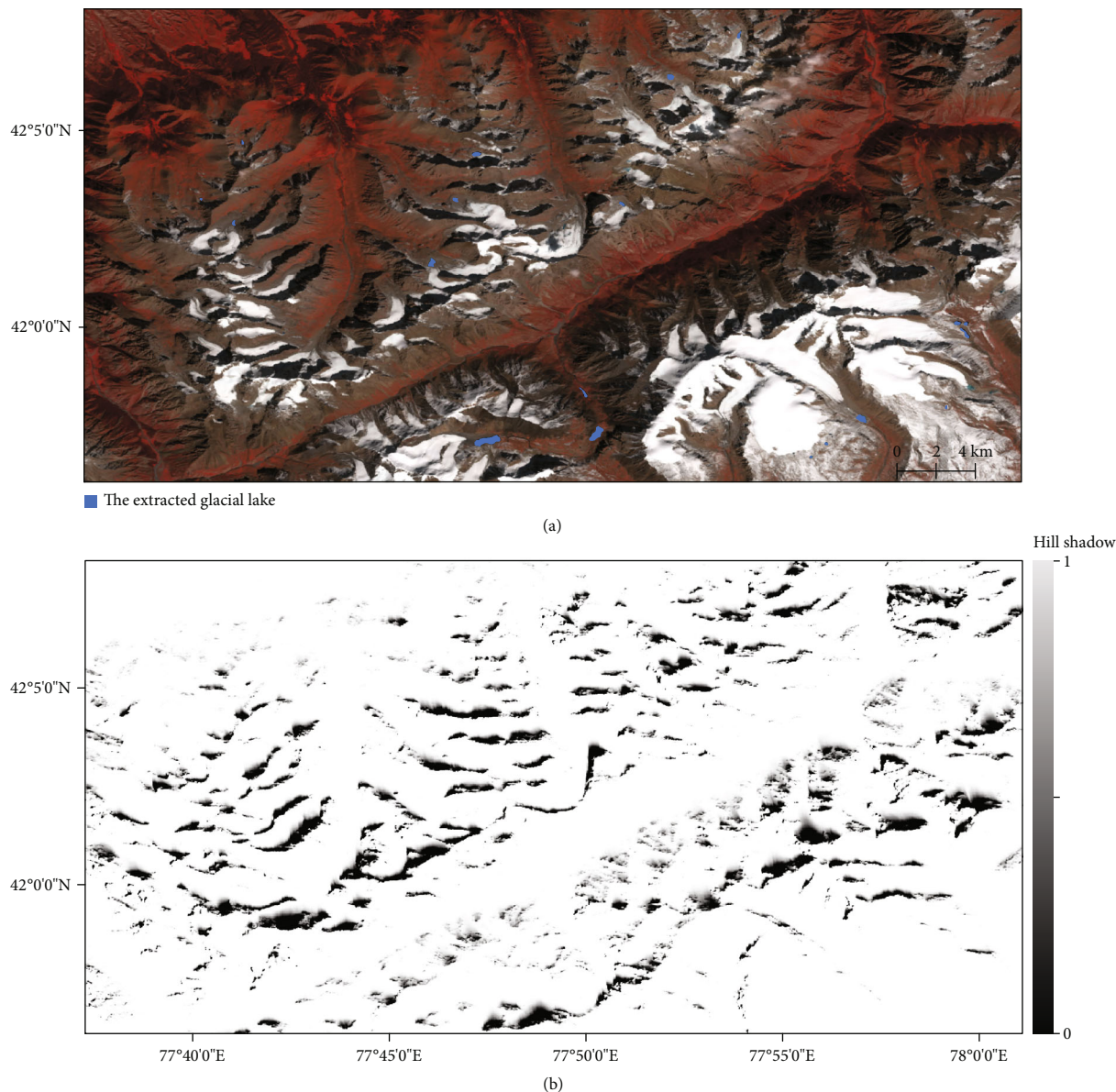


FIGURE 9: Hill shadow results in West Tien Shan in 2020. (a) Landsat 8 OLI image is acquired on September 26, 2020, with extracted glacial lakes shown in blue; (b) mean hill shadow map calculated using the image collection (images in warm seasons during 2018–2021) in GEE. The lower the value, the higher the probability of being a hill shadow.

in-depth exploration. There are large glacial lake regions extracted by our proposed method which were not digitized as glacial lakes in the inventory. These regions are mostly distributed on the debris-covered ablation zones of glaciers below 3500 m. Our mapped glacial lake areas have a high degree of confidence, and the valid observation times of each pixel are usually higher than 10, meaning that they are not ephemeral water bodies and may exist throughout several warm seasons. In our opinion, this overestimation is acceptable due to the different definitions for glacial lake mapping and producer’s operation. The substantial melting of glacier ice and snow was detected by our method (Figure 8(a)). Although they appeared as very shallow water with no clear water boundaries, they originated from glaciers and may be converted to

supraglacial or proglacial lakes in the short term [5, 58]. Moreover, most of the water ponds lie on the low-altitude glacier tongue in our extracted results (Figure 8(b)), but in the glacial lake inventory in HMA from Wang et al. (2020), the highly dynamic seasonal supraglacial lakes that have relatively small sizes, complex shapes, and large quantities (even hundreds of supraglacial ponds on a glacier terminus) that are not easily digitized were partially excluded. They are the main cause for the large disagreements between the extracted glacial lake extent using our automated method and glacial lake inventory from Wang et al. (2020).

Additional comparisons in the total number, total area, and maximum/minimum area of glacial lakes with Wang et al. (2020) and Chen et al. (2021) are listed in Table S1.

TABLE 2: Information of the datasets used in this study.

| Dataset                              | Temporal coverage | Spatial resolution | Data type                 | Source  |
|--------------------------------------|-------------------|--------------------|---------------------------|---|
| Landsat imagery                      | 1990 (1988–1993)  | 30 m               | Landsat 5/TM, tier 1 TOA  | United States Geological Survey (USGS)<br><a href="https://earthexplorer.usgs.gov">https://earthexplorer.usgs.gov</a>   |
|                                      | 2000 (1998–2003)  | 30 m               | Landsat 5/TM, tier 1 TOA  |   |
|                                      | 2010 (2009–2012)  | 30 m               | Landsat 5/TM, tier 1 TOA  |   |
|                                      | 2020 (2018–2021)  | 30 m               | Landsat 8/OLI, tier 1 TOA |   |
| SRTM DEM                             | 2000              | 30 m               | Single-raster band        | USGS <a href="https://http://earthexplorer.usgs.gov">https://http://earthexplorer.usgs.gov</a>  |
| TanDEM-X                             | 2018              | 1.7-3.5 m          | Single-raster band        | Apply from German Aerospace Center (DLR)<br><a href="https://tandemx-science.dlr.de/">https://tandemx-science.dlr.de/</a>                                       |
| RGI v6.0<br>Region 13–15             | 1999–2010         | —                  | Multipolygon shapefile    | Global Land Ice Measurements from Space (GLIMS) <a href="https://www.glims.org/RGI/rgi60_dl.html">https://www.glims.org/RGI/rgi60_dl.html</a>                   |
| GAMDAM glacier inventory             | 1990–2010         | —                  | Multipolygon shapefile    | See Sakai (2019)  |
| CRU v4.05                            | 1990–2020         | 0.5°               | Gridded dataset           | <a href="https://crudata.uea.ac.uk/cru/data/hrg/">https://crudata.uea.ac.uk/cru/data/hrg/</a>   |
| GPCC, full data monthly version 2020 | 1990–2019         | 0.25°              | Gridded dataset           | <a href="https://opendata.dwd.de/climate_environment/GPCC/html/download_gate.html">https://opendata.dwd.de/climate_environment/GPCC/html/download_gate.html</a> |

The statistics derived from our mapped glacial lakes are close to that of the inventory from Wang et al. (2020) for the epochs ~1990 and ~2020. We found that thousands of glacial lakes with a total area of about 300 km<sup>2</sup> were not detected by Chen et al. (2021). The main reasons for the missed glacial lakes in the inventory from Chen et al. (2021) are because of the interference of some bad observations (clouds or snow), drying up of small glacial lakes, or outburst in a single year [11].

### 2.6. Comparison of Lake Area Changes with Previous Studies.

The studies about observations of glacial lake area changes in the whole HMA region are very limited and only focus on the two time periods [9, 10]. To fully validate our results in other periods, in this section, the detailed comparisons were performed using the reported data of glacial lake area changes for parts of HMA and time intervals. The wide area increases were documented in mountains such as Pamir, South and East Tibet, and Hengduan Shan during 1990–2010 [59–61]. In our extracted results, glacial lake areas in Pamir, South and East Tibet, and Hengduan Shan increased  $0.58 \pm 0.15\%/a$ ,  $0.44 \pm 0.11\%/a$ , and  $0.47 \pm 0.19\%/a$  from 1990 to 2010, respectively. The large-scale retreat and melting of glaciers is thought to be the major cause for the rapid expansion of lake area in these regions [13, 56]. In Inner Tibet, glacial lakes were reported to expand 0.86%/a during 1990–2000 [31]; in our results, glacial lakes increased  $0.69 \pm 0.22\%/a$  during this period. For the whole Himalayan mountain range, we conducted a comparison between our results and the results from automatic extraction methods and human inspection during 1990–2015 [33]. In Nie et al.’s work, although each of the West Himalaya, Central Himalaya, and East Himalaya has been further divided into the northern side and southern side regions along the ridge line, respectively, it can be clearly shown that Central Himalaya expanded fastest, followed by the East Himalaya and West Himalaya over the past nearly three decades. This is similar to the results obtained by our method. Additional

comparisons for different subregions and time intervals are listed in Table 1.

Although the area coverages are different, our results are consistent with previous results in most subregions and periods (Table 1). The time of the data in the collected references is usually close to the periods covered by our results. There are three possible reasons for the severe deviations in some subregions. In the Hindu Kush and Karakoram, the observed opposite trends of glacial lake changes from our results, and the reference data are possibly caused by the very small study area in the reference and the wide existence of surge-type glaciers in this region. Glacial lakes in East Kun Lun are small and very sparsely distributed; the different observation periods and lakes smaller than 0.01 km<sup>2</sup> ignored by Zheng et al. (2021) may cause the differences in the results. In East Tien Shan, the large disagreement may stem from the snowy and rainy weather in areas above 3000 m, where ancient glacial deposits have also accumulated, seriously hindering the identification of glacial lakes. In the next section, we will discuss in more details about the influences of nonglacial lake areas on the mapping procedure.

## 3. Discussion

### 3.1. Influence of Snow and Ice.

Most of the previous studies adopted visual interpretation and digitalization to delineate glacial lakes. Although snow/ice meltwater can be effectively excluded, lakes that are completely covered by snow or ice are still difficult to recognize from individual satellite image [42]. In this paper, we used a three-step strategy to identify frozen or snow-covered glacial lakes. First, Landsat images in the warm seasons are used. Second, glacial lakes might be covered with snow or ice many times, while over an ~five-year period, glacial lakes can be identified based on the stable status of water bodies ( $NDWI > 0.1$ ). Third, the observation times for most of the regions in HMA are greater than 10, which improves the reliability of multitemporal glacial lake mapping results.



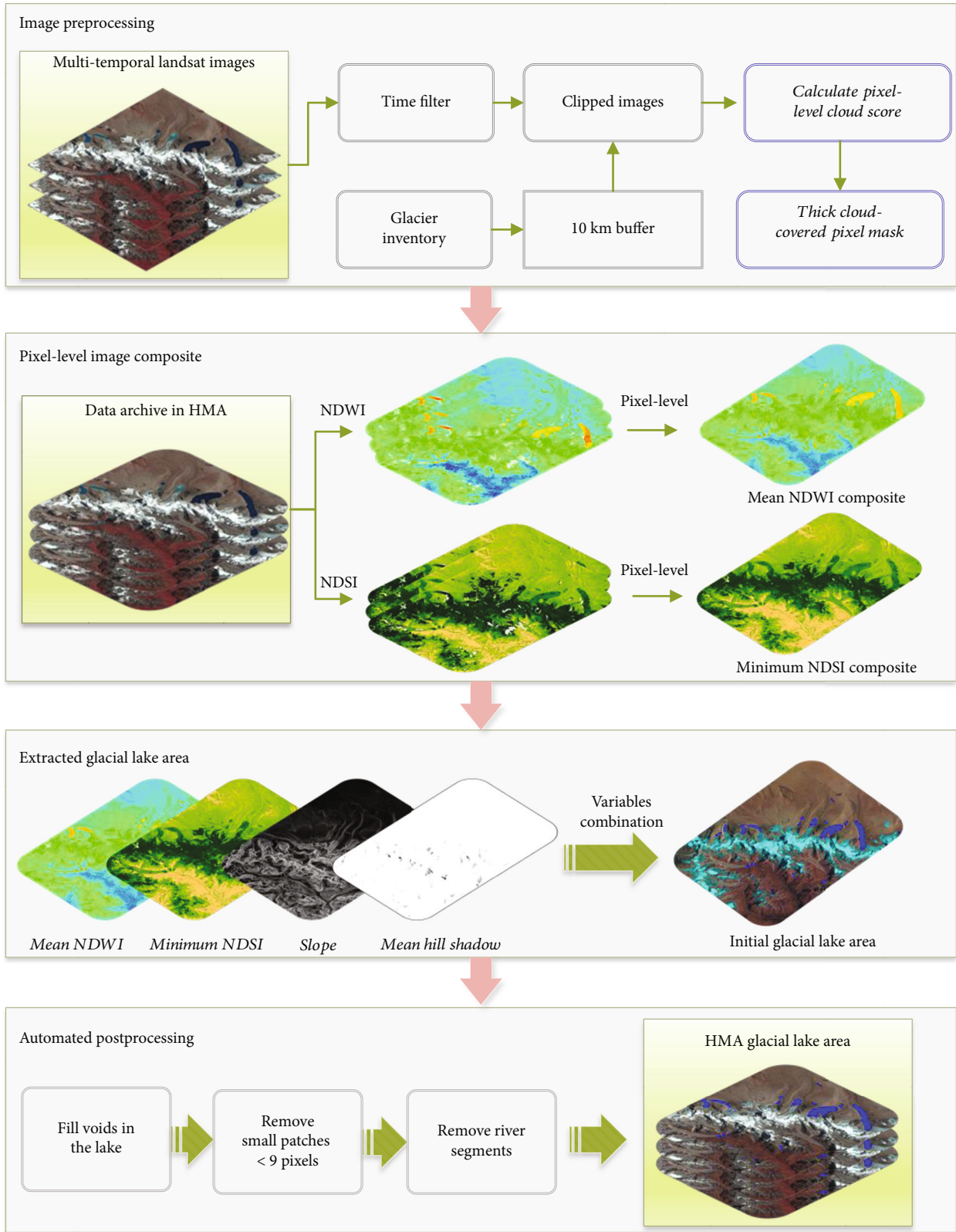


FIGURE 10: Flowchart of the processing chain for automated glacial lake detection.

The proposed method shows good performance for the large-scale glacial lake extraction even in the monsoon-affected areas with heavy cloud cover; e.g., Hengduan Shan

and South and East Tibet, their differences with the glacial lake inventory are less than 5% (Figure 7). In Central Himalaya, it was also found that there is a wide coverage of supraglacial

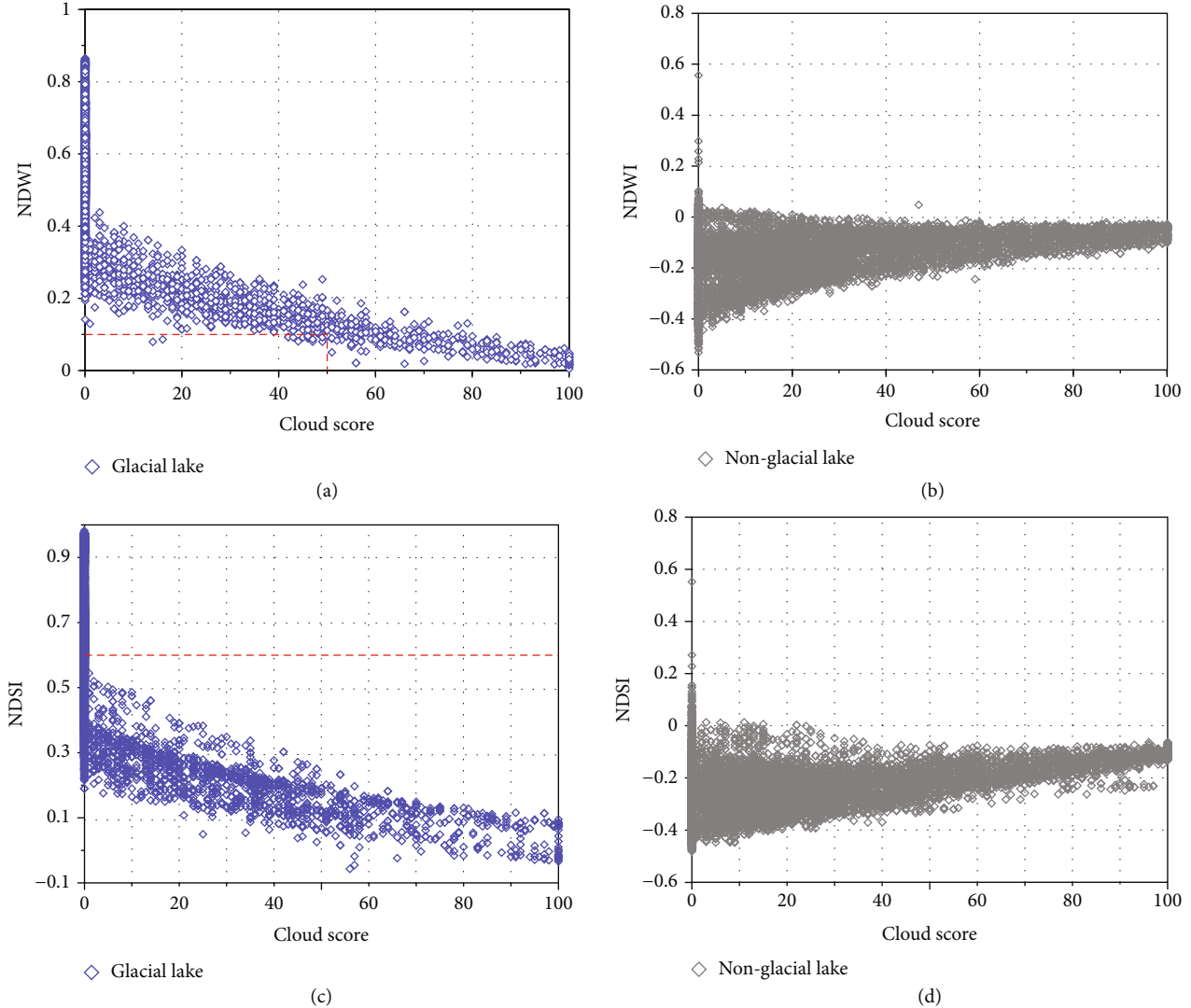


FIGURE 11: Relationship between cloud score, NDWI, and NDSI value for (a, c) 11,715 glacial lake pixels within the lake inventory boundaries and (b, d) 12,819 nonglacial lake pixels, all of which are selected visually from Landsat images in Karakoram and Central Himalaya with varying degrees of cloud cover.

ponds or snow/ice meltwater that were not delineated as glacial lakes in the inventory (Figure 8). Therefore, to reduce the bias for the estimation of glacial lake area changes, we take the intersection areas of our extracted glacial lakes with glacier boundaries as the uncertainty area. At present, however, we think it is difficult to resolve the discrepancy between our results and manual inventory since variation in the snow or ice melt contributions is hardly ignored during the automatic extraction over such a large area.

**3.2. Influence of Topographic Shadow.** The influence of topographic shadow in mountainous area is still a common problem for the delineation of glacial lakes or glaciers. Topographic parameters like shaded relief and slope are usually employed to distinguish between terrain shadows and lakes [11, 50]. However, the influence of terrain shadow cannot be completely eliminated due to the insufficiently detailed topographic features and time lag of DEM data.

The shadow area in the remote sensing image is mainly determined by the sun elevation and topography when the image is collected. In HMA, the areas seriously affected by the terrain shadows are the mountains with east–west ridges or near east–west ridges, such as the Tien Shan Mountains (Figure 9(a)), for which glaciers typically appear along the northern slope [40]. To greatly reduce topographic shadow, imagery collected from September to October is preferentially used because the solar elevation angles are relatively high. In our case, we fully consider the topographic relief, solar azimuth, and zenith synchronous with the image acquisition and use the mean value of the hill shadow for each time-series pixel set to alleviate shadowing effect (Figure 9(b)). It should be noted that the areas of the shadowed surface are different over different regions and even in the same region are different at different times, but generally, the remaining shadowed surface after the processing using the slope and mean hill shadow occupies a very small

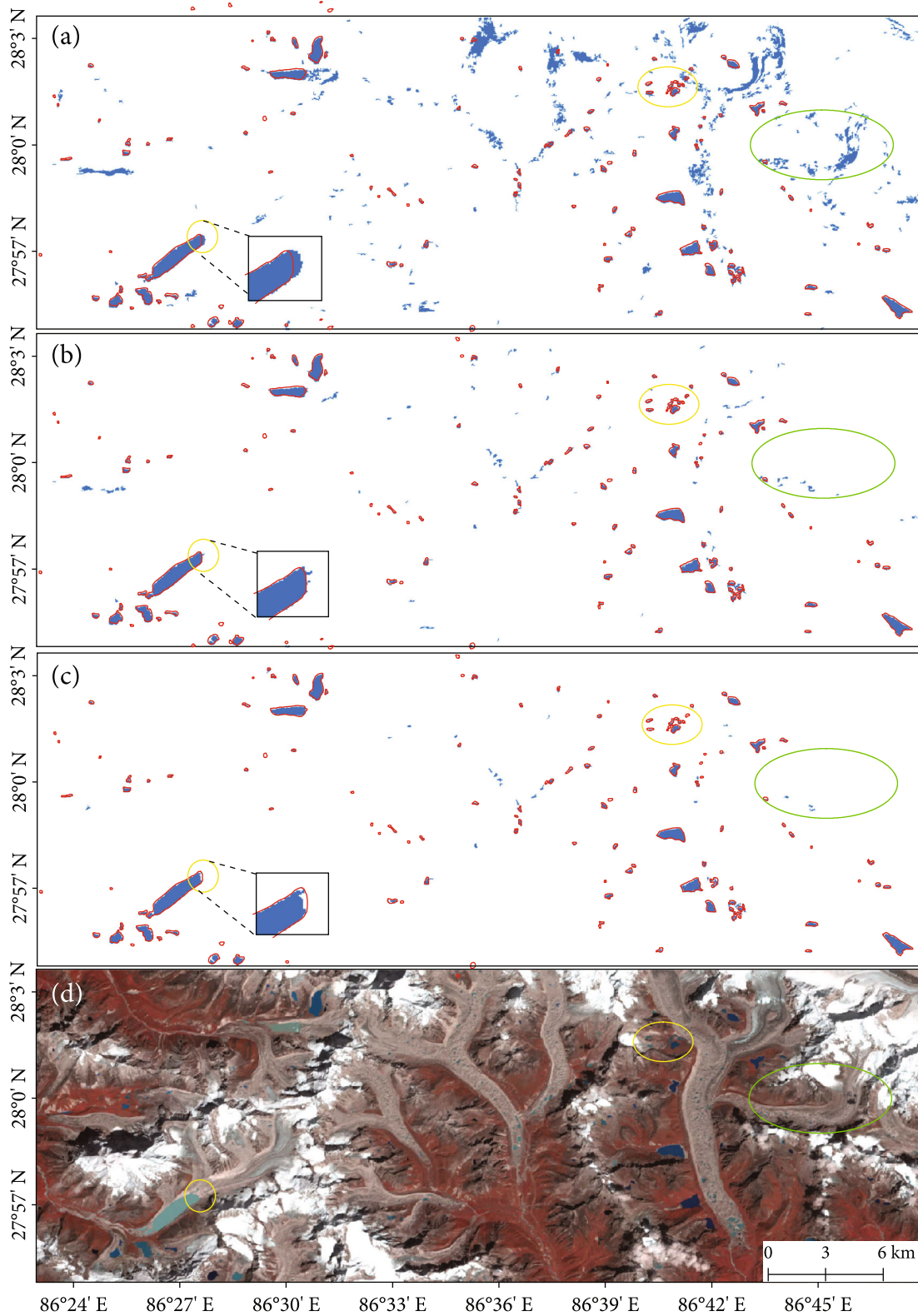


FIGURE 12: Glacial lake extraction images applying NDWI at (a) 0.05, (b) 0.1, and (c) 0.15 with NDSI at 0.6 in the East Himalaya in 2020. (d) is the corresponding false color composite of the Landsat 8 OLI image on September 05, 2020. The extracted glacial lakes are shown in blue, and the red outlines are the 2018 glacial lake inventory delineated by Wang et al. (2020). The areas within the yellow ellipses are considered as glacial lakes in the inventory, but using different thresholds of NDWI, parts of the area are not identified as glacial lakes. The areas within the green ellipses are areas outside the inventory, while some may actually be omitted by the inventory, and some might be identified as glacial lakes after applying different thresholds.

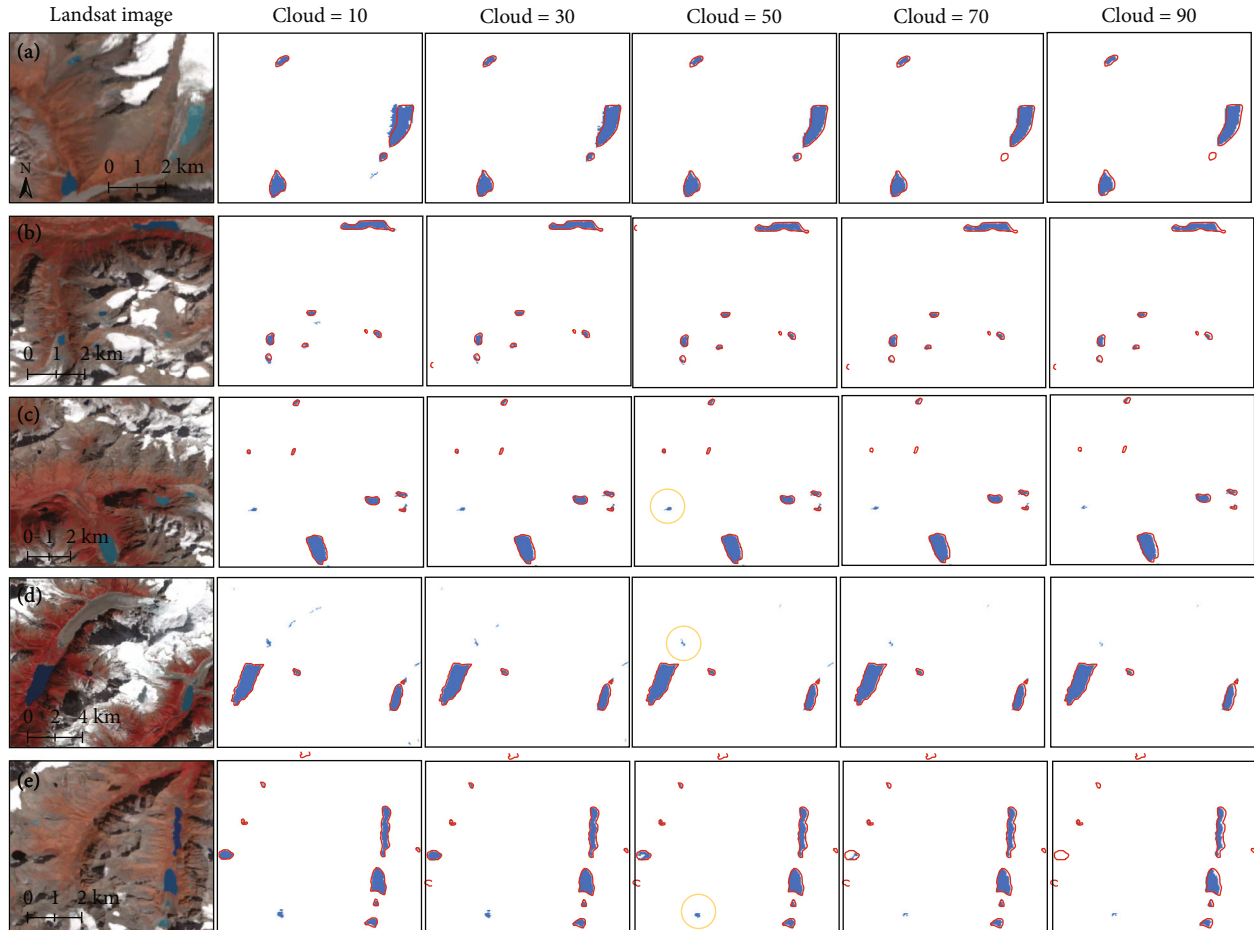


FIGURE 13: Experiments for different thresholds of cloud score (cloud score is set to 10, 30, 50, 70, and 90) on the composited image of 2020 at five test sites in the South and East Tibet. Glacial lakes extracted by our method are shown in blue color, and red outlines show the glacial lake inventory in 2018 (Wang et al., 2020). The regions in yellow ellipses are the lakes not identified by the glacial lake inventory. The central longitude and latitude of the five sites are (a) 93.5182°E, 30.4753°N; (b) 93.4925°E, 30.4092°N; (c) 93.4610°E, 30.2945°N; (d) 94.1435°E, 30.1417°N; and (e) 93.2521°E, 30.1124°N.

proportion in the final extracted lakes and will seldom affect the estimation of glacial lake area changes after subtraction of different periods.

### 3.3. Limitations and Advantages of the Proposed Method.

Multitemporal image composite was necessary for the low-quality images affected by thick clouds, frozen and snow-covered lakes, and topographic shadows. Glacial lake extent extracted using our automated method fits the real boundaries of the glacial lakes very well (Figure S4), while manually delineated glacial lake outlines are largely influenced by people's subjective experience and manual operation, resulting in inaccurate extraction of lake details near the glacier terminus and overestimation or complete omission of some small glacial lakes. Moreover, manual digitization shows poor performance for the delineation of glacial lakes with complex curved shapes.

Apart from manual delineation, many automatic methods were proposed for the glacial lake extraction. Thresholding segmentation method is simple but effective

for the small homogeneous area [9, 19, 33, 40], while for a large region with diverse environment, the classification accuracy will be greatly reduced. To improve the details of lake edge, level-set-based active-contour approaches fully consider the regional heterogeneity and can be applicable to different features [15, 22, 65, 66]. However, the calculation is complicated, and many attempts are needed to select optimized parameters. Object-oriented classification methods fully exploit the lake spectral information, morphological characteristics, and contextual information [21, 23]. The main limitation lies in the manual establishment of classification rules and segmentation scales. The improved deep learning methods have high automation for detecting glacial lakes without assistance of additional auxiliary data [24–26, 67], while enough and representative training samples are required.

In comparison with these automatic glacial lake mapping methods, our method has the following advantages: (1) The method was developed based on the GEE cloud computing platform which offered massive images for the high-efficiency



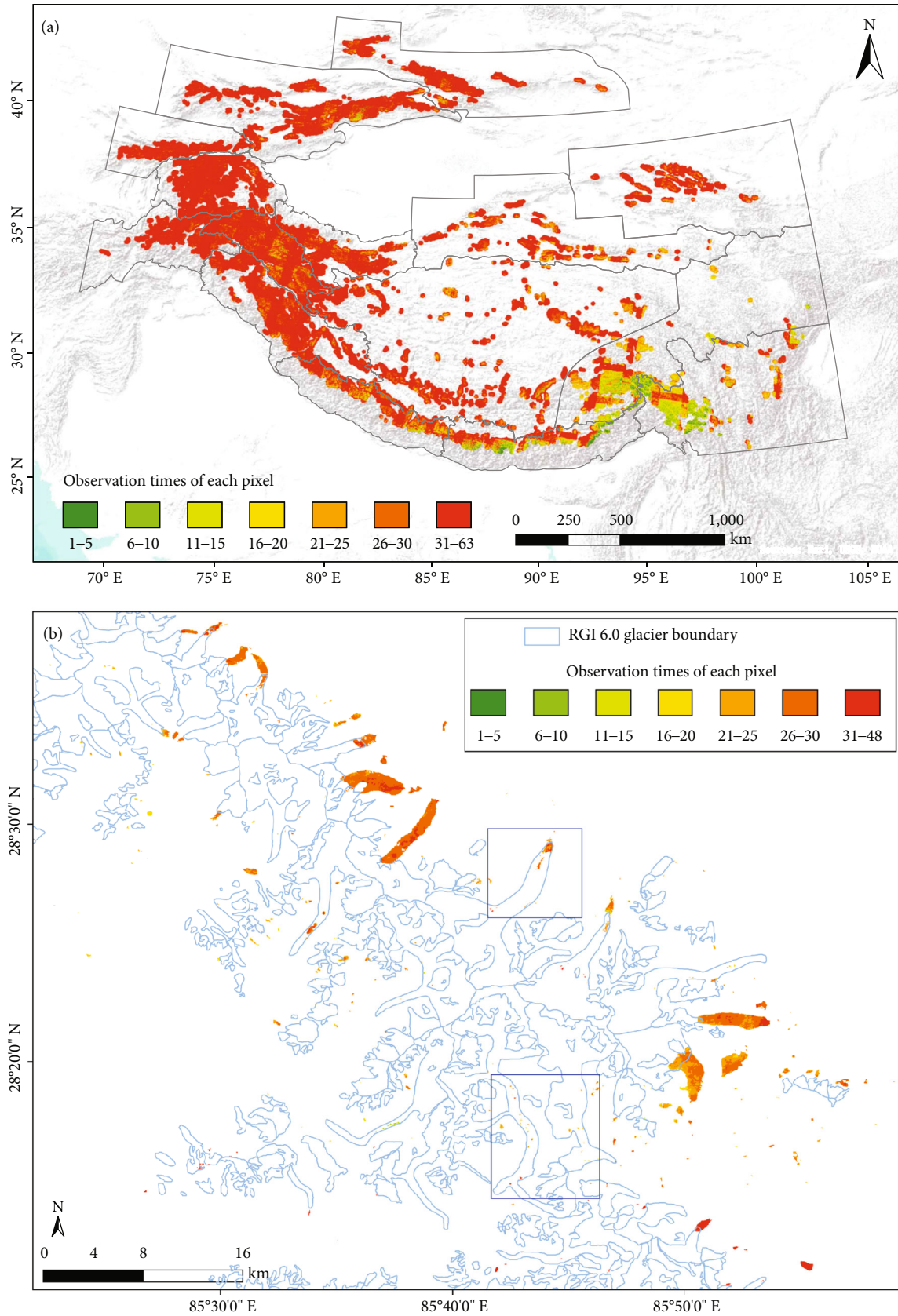


FIGURE 14: (a) Map of observation times per pixel after cloud filtering for the glacier-buffered regions in HMA. Black polygons represent the extent of subregions. (b) Lake-specific mapping times in the Central Himalaya in 2020. Two blue boxes mark the location of maps enlarged in Figure 8.

pixel-level composite. (2) It is unnecessary to select available data from a large number of images and then merge them; all images can be fully utilized to obtain a pixel-level composited glacial lake map. (3) The impacts of ice, snow, cloud, and hill shadow were comprehensively considered and greatly removed; the evaluation indicators were established to reduce the impact from glacial meltwater on the mapping results. (4) Our method shows high accuracy for the extraction of the lake details and can capture areas of tiny supraglacial and unconnected glacial lakes that are easily overlooked.

However, there are also some limitations in the proposed method. The main problem with compositing images over ~5 years is that in regions where glacial lakes change extremely rapidly, the edges of glacial lakes will look “blurred.” For the few highly active glacial lakes, e.g., Lake Merzbacher in Tien Shan, which has suddenly breached nearly every year due to intense glacier melting or huge ice falling into the lake [8], our method is not able to capture rapid changes and ensuing GLOF events over the entire growing period of such glacial lakes. That is the main limitation of this methodology in detecting glacial lake changes, which only considers most of glacial lakes that evolve stably or slowly.

Another problem with our proposed method is that we consider all the lakes within this 10 km buffer zone to be glacial lakes, which is controversial and may cause deviations since nonglacier-fed lakes were regarded as nonglacial lakes in some studies [31, 32]. Examples of the deviations caused by the nonglacial lake pixels in typical regions are shown in Figure S5. It can be seen that nonglacial lakes bring great uncertainty to the total number and area of glacial lakes in the East Himalaya. The number of nonglacial lakes accounts for nearly half of the total number; the area accounts for a slightly lower proportion, about 18%. The errors caused by the nonglacial lake area in West Tien Shan and West Kun Lun decreased, occupying 8% and 2% of the total lake area, respectively. More deviations of number were observed for the West Tien Shan, with nonglacial lakes accounting for about 18% of the total number. Generally, the errors caused by the nonglacial lake pixels are different in different mountains, and the resulting errors of area are smaller than that of the number.

In the mapping results, glacial lakes directly in contact with glaciers or lying on the glacier surface were identified; however, some glacial meltwater at the glacier terminus was also extracted with high confidence (the observation times were usually >10), excluding the possibility of transient meltwater (Figure 8). This glacial meltwater can exist for several warm seasons and will continue to accumulate or flow downward [68]. Traditional methods using human vision have difficulty in distinguishing glaciers from glacial meltwater, but glacial meltwater can be quickly differentiated using our proposed method. Although this continuous melting of snow and ice has not yet evolved into a stable water body and has not been taken as glacial lake in the manually delineated inventory, in our opinion, it is more sensitive to the climatic warming than glacier itself due to the thermal effect and offers new perspectives for understanding the glacier mass loss and glacial lake formation.

## 4. Conclusion

No systematic studies have been made to investigate the current distribution and long-term heterogeneous changes of glacial lakes in the whole HMA. Glacial lake mapping from satellite images is of crucial importance for glacial lake dynamics monitoring. In previous studies, the heavy clouds, snow or ice cover, and terrain shadows were the major obstacles for image selection from a large number of images and accurate lake mapping. This study is aimed at solving these problems by developing a new automated glacial lake extraction method. First, due to the spectral complexity and multiple influencing objects in alpine environments, the multitemporal mean NDWI composite was proposed for the stable glacial lake extraction. Then, different cloud scores and NDSI settings were tested in this study, and shadowed pixels were greatly reduced using the mean hill shadow > 0.9. The uncertainties from supraglacial lakes and glacial meltwater were estimated using the intersection area between the extracted results and glacier inventory boundaries. The strength of this method is that we composite the glacial lake image at the pixel level by making full use of all the available images, rather than just image mosaicking.

Glacial lake area changes present successive and consistent increases in the past 30 years. The estimated glacial lake area increase was  $0.58 \pm 0.21\%/a$  ( $8.57 \pm 3.16 \text{ km}^2/a$ ) in HMA from 1990 to 2020, showing strong spatiotemporal heterogeneity of changes. The fastest expanding area of glacial lake was East Kun Lun, and its growth rate was  $2.01 \pm 0.54\%/a$ . Pamir and Hengduan Shan have the slowest increases, which were  $0.33 \pm 0.08\%/a$  and  $0.39 \pm 0.01\%/a$ , respectively. Even in the glacier accumulated regions—West Kun Lun—the glacial lake area increased to some extent due to the dominant effects from the increased precipitation. The greatest expansion occurred at 5000–5200 m a.s.l., with the increased area of about  $45 \text{ km}^2$  (~25%). The warming temperature and thinning glaciers are considered to be the main drivers of widespread glacial lake expansion in HMA region. The long-term glacial lake dataset, proposed automated glacial lake mapping method, and findings in this study have important implications to improve the understanding of glacial lakes and glacier hydrological changes, as well as for disaster risk assessment in mountainous glaciated regions.

## 5. Materials and Methods

**5.1. Datasets.** Approximately 30,000 Landsat Thematic Mapper (TM) and Operational Land Imager (OLI) scenes were accessed from GEE for the lake mapping in the periods of 1990, 2000, 2010, and 2020. The ten-year interval between these four periods is chosen to fully explore the changes in glacial lakes during the past decades. Because the high-quality images in a single year are quite limited in HMA, to obtain abundant data, all available images were collected within  $\pm 2\sim 3$  years of the four periods (Table 2). Landsat 8 shows better performance for the lake mapping compared with its previous sensors due to the enhanced image acquisition technology and improved sensor [69]. The archived

Landsat 5 images are fewer than those of Landsat 8, and thus, the selected time span for 1990 and 2000 is relatively long. Landsat Tier 1 calibrated top-of-atmosphere (TOA) reflectance images on GEE were employed.

Other auxiliary dataset are as follows: (i) Randolph Glacier Inventory (RGI v6.0) [30] to delimit the distribution of glacial lakes within its 10 km buffer. An updated glacier inventory—Glacier Area Mapping for Discharge from the Asian Mountains (GAMDAM) [70]—has also been included to supplement some missing glaciers in RGI v6.0. (ii) HMA glacial lake inventory for comparison and cross-validation of our results [10]. (iii) Version 3.0 Shuttle Radar Topography Mission (SRTM) DEM with approximately 30 m resolution to reduce the effect of terrain shadows on glacial lake mapping and combined with TanDEM-X data acquired in 2018, to calculate the glacier thickness changes (TanDEM-X minus SRTM DEM). (iv) Monthly gridded temperature dataset derived from Climate Research Unit (CRU) data (v4.05, 0.5° spatial resolution) to estimate the temperature changes in HMA from 1990 to 2020. (v) Monthly land-surface precipitation data from Global Precipitation Climatology Centre (GPCC) with a spatial resolution of 0.25° to estimate the precipitation trend in HMA during 1990–2019.

## 5.2. Methodology

**5.2.1. The Processing Chain.** To automatically detect glacial lakes from Landsat time series of images while overcoming the limitations of clouds, terrain shadows, and seasonal snow or ice cover, our proposed method composites a glacial lake map on pixel scale, which mainly consists of four steps (Figure 10): (1) image preprocessing to filter out the frozen season images, nonglacial lakes, and thick cloud-covered pixels; (2) multitemporal mean NDWI composite and minimum NDSI composite; (3) glacial lake area extraction; and (4) automated postprocessing step.

**(1) Image Preprocessing.** To minimize the influences from seasonal snow or ice cover, images were mostly selected in the warm season (June to November) for the four periods. During this time, the lakes also featured the most stable and maximum extent following glacier ablation. In monsoon-affected regions such as Southeastern Tibet and Central and Eastern Himalaya, late September to November is more suitable due to the abundant monsoon cloud cover in summer. We reduced the search range to <10 km of glacier terminus in the inventory and considered all the mapped lakes within this range as glacial lakes [10, 33]. We excluded areas far from each glacier, assuming that plateau lakes in these regions have weak interactions with glaciers.

Time series of clipped Landsat images in HMA make up pixel sets at each pixel location. Then, the cloud score (in the range [0, 100]) of each pixel is calculated using the Landsat simpleCloudScore function provided by GEE based on a combination of brightness, temperature, and NDSI. For the cloudy areas, the absolutely clear-sky pixels (cloud score equals zero) are too limited to composite a glacial lake map. We found that water covered by thin clouds can be separated from the land and still

be identified as water pixels. Here, we used 11,715 pixels of lakes located within the boundaries of glacial lake inventories from Wang et al. (2020), pixels that may be cloudy or clear; it was observed that NDWI decrease with the increase of cloud score (Figure 11(a)). For glacial lake pixels with cloud scores less than 50, their NDWI is higher than 0.1, the threshold within the range of 0.05 to 0.15 for glacial lake mapping [19, 22]. The results for nonglacial lake areas show no obvious trend (Figure 11(b)), but the NDWI is mostly lower than 0, indicating that nonglacial lake pixels are less likely to be recognized as glacial lake pixels due to the cloud score settings. Some glaciers connected to glacial lakes can be misclassified as lakes using only NDWI; thus, NDSI was utilized for the further glacial lake identification. The NDSI of most lake pixels is lower than 0.4 (Figure 11(c)), a threshold that is generally used for the extraction of glacier coverage area [49, 71]. Almost all pixels are lower than 0.6, which may be more reasonable for the exclusion of glaciers while extracting lake water bodies that are sometimes partially covered with ice or snow. The NDSI of nonglacial lake regions is insensitive to the cloud score, similar to the results of NDWI (Figure 11(d)). Based on the above analysis, we used a threshold of 50 on the cloud score to mask thick cloudy pixels. A very low cloud score threshold will reduce the available pixel sets, and seasonal snow and ice melt will be misclassified as glacial lakes, resulting in overestimation of lake area. A very high threshold will include thick cloud pixels, which will be identified as land pixels no matter the clouds are over land or water [72], making the lake area underestimated.

**(2) Pixel-Level Image Composite.** This step is aimed at calculating the NDWI and NDSI values for each pixel of the images after the cloud mask and then composite new images with the mean NDWI value and minimum NDSI value for each pixel set. The mean NDWI value represents the stable status of lake pixels, and it can obtain complete interior pixels of lake water to the greatest extent. The minimum NDSI is helpful for the exclusion of snow or ice cover when the exposed glacier is undergoing ablation during the observation time.

**(3) Glacial Lake Area Extraction.** According to the above experiments and related studies [19, 22], glacial lakes in the Tibetan Plateau have NDWI values higher than 0.05 or 0.15 using Landsat images. Here, we set the threshold of NDWI to 0.1 to extract glacial lakes from the composited image. To avoid commission errors from the glacier and, at the same time, retain the lakes partly covered by seasonal snow or bare ice, 0.6 is used as the threshold on the minimum composited NDSI image. A slope threshold of <20° [9] is employed to alleviate disturbances from terrain shadows. Moreover, shadow of each pixel set is calculated using the hillShadow algorithm in GEE taking the input of the DEM, solar azimuth, and zenith of the image, with an output of 1 where pixels are illuminated and 0 where they are shadowed. In this study, pixels with mean hill shadows higher than 0.9 are considered illuminated regions given the transient appearance of shadows on the time scale. By synthesizing from the former conditions, binary images of glacial lakes in HMA are obtained.



(4) *Automated Postprocessing.* In the binary image, some of the holes exist within the lakes due to the heterogeneous spectral responses from variable suspended solids, water depth, and colored dissolved materials in the water. In a postprocessing step, we search the connected void pixels in the existing lake region and fill them and remove small patches  $< 9$  pixels ( $0.0081 \text{ km}^2$ ) that originate from noise from unstable tiny ponds and river segments [11]. Finally, the time series of glacial lake maps are generated. This method has a high degree of automation for the glacial lake extraction. Given the amount of work required to update the inventory and improve the work efficiency of large-scale glacial lake dynamic monitoring, while minimizing the influence of subjective judgment of operators, each glacial lake boundary was not visually checked and reedited with original Landsat images.

5.2.2. *Tests of Optimal NDWI Threshold.* In HMA, glacier backgrounds dominate the scenes. Therefore, both NDWI and NDSI are applied sequentially: firstly, NDWI is applied to extract the water bodies from images; then, NDSI is used to eliminate the pixels misclassified with glaciers. Since NDWI is designed to separate water and nonwater types, it forces water types above 0 and nonwater types below 0; some thresholds above 0 (e.g., 0.05 or 0.15) are applied to extract glacial lakes from NDWI images. However, due to the varying brightness and contrast of the scene with space and time, these thresholds might not always achieve the best classification accuracy. In this section, multiple thresholds of NDWI were considered to determine the optimal threshold, which approximates to the minimum sum of commission and omission errors.

A comparison of the glacial lake extraction results using different thresholds of NDWI is shown in Figure 12 as an example. The glacial lake outlines in 2018 [10] generated by satellite images from 2016 to 2020 were taken as a reference. Obviously, the threshold of NDWI at 0.05 (Figure 12(a)) overestimated the lake area; although most areas within the inventory boundaries are identified as glacial lakes, in the regions outside the inventory boundaries, large portions of glacier terminus are also mistakenly recognized. If the threshold of NDWI is set to 0.15 (Figure 12(c)), the influence of glaciers is greatly reduced, but many small glacial lakes are not detected, and there are missing pixels on the lake edge. This implies that 0.1 (Figure 12(b)) could be reasonable to classify glacial lakes under various environmental conditions, with a tradeoff between commission and omission errors. The choice of the multitemporal pixel-level image composite scheme also intends to stabilize this threshold.

5.2.3. *Tests of Cloud Score Thresholds.* The use of different thresholds of the cloud score directly controls the number of available pixels in each pixel location; thus, it is important for the final glacial lake extraction. An example of the influence of different cloud score thresholds on glacial lake extraction is presented in Figure 13. In HMA, South and East Tibet is one region most vulnerable to cloud cover, so the composited image in 2020 in the South and East Tibet region is selected as an example. Generally, most glacial lakes can be identified using this pixel-level composite strategy regardless

of the cloud score. It can even automatically extract previously undiscovered glacial lakes (shown in the yellow ellipses). When the threshold of cloud score is below 50, clouds have little impact on glacial lake extraction. Most pixels in the inventory boundaries are delineated, but many pixels of snow or ice are misclassified as glacial lakes. When the cloud score is higher than 50, thick clouds block all information for land (including snow and ice) and water separation, and glacial lake extraction is prone to be underestimated together with the absence of small glacial lakes. The cloud score should therefore be set to 50 to ensure a satisfactory amount of the pixel sets used and high extraction accuracy.

5.2.4. *Uncertainties of Snow or Ice Melt.* Glacial lake area could be overestimated due to the melting of ice or snow on the glaciers if the data were found to be insufficient (Figure 13). Here, the mean NDWI value of pixel set is taken as corresponding value of composite images, meaning that if seasonal meltwater has been short-lived, those pixels would not be recognized as glacial lakes. We also calculated the observation times of each pixel used in the production of the multitemporal mean NDWI composite and minimum NDSI composite, which records how many valid pixels in each pixel location can be used to determine whether a pixel is a glacial lake during the observation period (Figure 14(a)). The observation times are high on most occasions because the data were collected during ~5 warm seasons (June to November) with a revisit cycle of 16 days for each mapping period (Table 2). However, in areas with frequent cloud cover, such as Himalaya and South and East Tibet regions, the observation times may be relatively low after the cloudy pixels are masked. Using the combination of NDWI and NDSI, most of the pixels of glaciers distributed downstream or around glacial lakes can be excluded, but there are still a few misclassified glacier pixels with sustained high water content, usually known as glacier and snow runoff. Figure 14(b) is taken as an example to show the observation times of each pixel in the mapped glacial lake areas in Central Himalaya. More observation times mean that glacial lakes can be more accurately extracted, but this also inevitably mixes with some high glacial meltwater pixels. To reduce noise and ensure the quality of glacial lake changes, one possible solution is to directly mask off glaciers using a glacier outline inventory. However, such work might also erase much of the information about supraglacial lakes that lie on the surface of glaciers. In this study, we take the intersection area of the glacier boundary and extracted glacial lake areas as qualitative measurement of area uncertainties, by fully considering the impact of glacial meltwater and the uncertainty caused by the high variability of the supraglacial lakes.

## Data Availability

The data used to support the findings of this study are included within the article and can be requested from the authors.

## Conflicts of Interest

The authors declare no competing financial interest.



## Authors' Contributions

Meimei Zhang and Fang Chen conceptualized the work; Meimei Zhang and Huadong Guo designed the experiment; Meimei Zhang, Lu Yi, and Jiangyuan Zeng processed the data and conducted the formal analysis; Lu Yi and Bin Li verified the results; Meimei Zhang and Fang Chen wrote the manuscript and revised it; Meimei Zhang and Fang Chen contributed equally to this work.

## Acknowledgments

This work was supported by the Strategic Priority Research Program of the Chinese Academy of Sciences (XDA19030101) and the National Natural Science Foundation of China (41871345).

## Supplementary Materials

Figure S1: changes in the area and number of glacial lakes for each 200 m elevation band in HMA region from 1990 to 2020: (a) area changes; (b) number changes. Figure S2: spatial pattern of temperature and precipitation changes in HMA: (a) trend in temperature change from 1990 to 2020 produced by CRU data (v4.05, 0.5° spatial resolution); (b) annual mean precipitation changes for the period 1990–2019 obtained from GPCP data (full data monthly version 2020, 0.25° spatial resolution). The symbol “+” indicates the linear fit of temperature/precipitation versus time is at the 90% confidence interval. Figure S3: glacier surface elevation changes in three typical glaciated areas of HMA during 2000–2018: (a) West Tien Shan; (b) West Kun Lun; (c) East Himalaya. The values in subplots represent the estimated mean glacier elevation changes in each region. Figure S4: example showing the mapped glacial lakes by our proposed method, Chen et al. (2021), and Wang et al. (2020) in the Central Himalaya in 2020. (a–d) represent four enlarged maps of glacial lakes. Background image is from false-color composited (bands: 5/4/3) Landsat-8 OLI image in October 2, 2020. Figure S5: examples showing the deviations caused by the nonglacial lake pixels: (a) geographic location of three typical regions; (b) number and area of all the mapped lakes and nonglacial lakes for typical regions in West Tien Shan, West Kun Lun, and East Himalaya. Table S1: comparisons between the two released HMA glacial lake inventories and glacial lakes mapped in this study. (*Supplementary Materials*)

## References

- [1] K. L. Cook, C. Andermann, F. Gimbert, B. R. Adhikari, and N. Hovius, “Glacial lake outburst floods as drivers of fluvial erosion in the Himalaya,” *Science*, vol. 362, no. 6410, pp. 53–57, 2018.
- [2] S. Kaushik, M. Rafiq, P. K. Joshi, and T. Singh, “Examining the glacial lake dynamics in a warming climate and GLOF modeling in parts of Chandra basin, Himachal Pradesh, India,” *Himachal Pradesh, India, Science of The Total Environment*, vol. 714, article 136455, 2020.
- [3] D. Farinotti, M. Huss, J. J. Fürst et al., “A consensus estimate for the ice thickness distribution of all glaciers on Earth,” *Nature Geoscience*, vol. 12, no. 3, pp. 168–173, 2019.
- [4] H. D. Pritchard, “Asia’s glaciers are a regionally important buffer against drought,” *Nature*, vol. 545, no. 7653, pp. 169–174, 2017.
- [5] C. S. Watson, O. King, E. S. Miles, and D. J. Quincey, “Optimising NDWI supraglacial pond classification on Himalayan debris-covered glaciers,” *Remote Sensing of Environment*, vol. 217, pp. 414–425, 2018.
- [6] S. Harrison, J. S. Kargel, C. Huggel et al., “Climate change and the global pattern of moraine-dammed glacial lake outburst floods,” *The Cryosphere*, vol. 12, no. 4, pp. 1195–1209, 2018.
- [7] G. Veh, O. Korup, S. von Specht, S. Roessner, and A. Walz, “Unchanged frequency of moraine-dammed glacial lake outburst floods in the Himalaya,” *Climate Change*, vol. 9, no. 5, pp. 379–383, 2019.
- [8] W. Furian, D. Loibl, and C. Schneider, “Future glacial lakes in High Mountain Asia: an inventory and assessment of hazard potential from surrounding slopes,” *Journal of Glaciology*, vol. 67, no. 264, pp. 653–670, 2021.
- [9] G. Zheng, S. K. Allen, A. Bao et al., “Increasing risk of glacial lake outburst floods from future Third Pole deglaciation,” *Nature Climate Change*, vol. 11, no. 5, pp. 411–417, 2021.
- [10] X. Wang, X. Guo, C. Yang et al., “Glacial lake inventory of high-mountain Asia in 1990 and 2018 derived from Landsat images,” *Earth System Science Data*, vol. 12, no. 3, pp. 2169–2182, 2020.
- [11] F. Chen, M. Zhang, H. Guo, S. Allen, and C. S. Watson, “Annual 30 m dataset for glacial lakes in High Mountain Asia from 2008 to 2017,” *Earth System Science Data*, vol. 13, no. 2, pp. 741–766, 2021.
- [12] C. Song, Y. Sheng, J. Wang, L. Ke, A. Madson, and Y. Nie, “Heterogeneous glacial lake changes and links of lake expansions to the rapid thinning of adjacent glacier termini in the Himalayas,” *Geomorphology*, vol. 280, pp. 30–38, 2017.
- [13] O. King, A. Bhattacharya, R. Bhambri, and T. Bolch, “Glacial lakes exacerbate Himalayan glacier mass loss,” *Scientific Reports*, vol. 9, no. 1, pp. 18145–18145, 2019.
- [14] J. Gardelle, Y. Arnaud, and E. Berthier, “Contrasted evolution of glacial lakes along the Hindu Kush Himalaya mountain range between 1990 and 2009,” *Global and Planetary Change*, vol. 75, no. 1–2, pp. 47–55, 2011.
- [15] H. Zhao, F. Chen, and M. Zhang, “A systematic extraction approach for mapping glacial lakes in High Mountain regions of Asia,” *IEEE Journal of Selected Topics in Applied Earth Observations and Remote Sensing*, vol. 11, no. 8, pp. 2788–2799, 2018.
- [16] S. K. McFeeters, “The use of the normalized difference water index (NDWI) in the delineation of open water features,” *International Journal of Remote Sensing*, vol. 17, no. 7, pp. 1425–1432, 1996.
- [17] H. Xu, “Modification of normalised difference water index (NDWI) to enhance open water features in remotely sensed imagery,” *International Journal of Remote Sensing*, vol. 27, no. 14, pp. 3025–3033, 2006.
- [18] G. L. Feyisa, H. Meilby, R. Fensholt, and S. R. Proud, “Automated water extraction index: a new technique for surface water mapping using Landsat imagery,” *Remote Sensing of Environment*, vol. 140, pp. 23–35, 2014.

- [19] J. Li and Y. Sheng, "An automated scheme for glacial lake dynamics mapping using Landsat imagery and digital elevation models: a case study in the Himalayas," *International Journal of Remote Sensing*, vol. 33, no. 16, pp. 5194–5213, 2012.
- [20] N. Otsu, "A threshold selection method from gray-level histograms," *IEEE Transactions on Systems, Man, and Cybernetics*, vol. 9, no. 1, pp. 62–66, 1979.
- [21] K. V. Mitkari, M. K. Arora, and R. K. Tiwari, "Extraction of glacial lakes in Gangotri Glacier using object-based image analysis," *IEEE Journal of Selected Topics in Applied Earth Observations and Remote Sensing*, vol. 10, pp. 5275–5283, 2017.
- [22] F. Chen, M. Zhang, B. Tian, and Z. Li, "Extraction of glacial lake outlines in Tibet Plateau using Landsat 8 imagery and Google Earth Engine," *IEEE Journal of Selected Topics in Applied Earth Observations & Remote Sensing*, vol. 10, no. 9, pp. 4002–4009, 2017.
- [23] A. M. Johansson and I. A. Brown, "Adaptive classification of supra-glacial lakes on the West Greenland Ice Sheet," *IEEE Journal of Selected Topics in Applied Earth Observations & Remote Sensing*, vol. 6, no. 4, pp. 1998–2007, 2013.
- [24] S. Wangchuk and T. Bolch, "Mapping of glacial lakes using Sentinel-1 and Sentinel-2 data and a random forest classifier: strengths and challenges," *Science of Remote Sensing*, vol. 2, article 100008, 2020.
- [25] R. Wu, G. Liu, R. Zhang et al., "A deep learning method for mapping glacial lakes from the combined use of synthetic-aperture radar and optical satellite images," *Remote Sensing*, vol. 12, no. 24, p. 4020, 2020.
- [26] M. Dirscherl, A. J. Dietz, C. Kneisel, and C. Kuenzer, "A novel method for automated supraglacial lake mapping in Antarctica using Sentinel-1 SAR imagery and deep learning," *Remote Sensing*, vol. 13, no. 2, p. 197, 2021.
- [27] A. Fisher, N. Flood, and T. Danaher, "Comparing Landsat water index methods for automated water classification in eastern Australia," *Remote Sensing of Environment*, vol. 175, pp. 167–182, 2016.
- [28] X. Yao, S. Liu, L. Han, M. Sun, and L. Zhao, "Definition and classification system of glacial lake for inventory and hazards study," *Journal of Geographical Sciences*, vol. 28, no. 2, pp. 193–205, 2018.
- [29] B. M. Sudan, K. M. Pradeep, L. Wu et al., "The status of glacial lakes in the Hindu Kush Himalaya-ICIMOD research report 2018/1," in: *ICIMOD Research Report*, 2018.
- [30] Rgi Consortium, *Randolph Glacier Inventory-a dataset of global glacier outlines: version 6.0*, Colorado, USA, 2017.
- [31] G. Zhang, T. Yao, H. Xie, W. Wang, and W. Yang, "An inventory of glacial lakes in the Third Pole region and their changes in response to global warming," *Global and Planetary Change*, vol. 131, pp. 148–157, 2015.
- [32] G. Zhang, T. Bolch, S. Allen, A. Linsbauer, W. Chen, and W. Wang, "Glacial lake evolution and glacier-lake interactions in the Poiqu River basin, central Himalaya, 1964–2017," *Journal of Glaciology*, vol. 65, no. 251, pp. 347–365, 2019.
- [33] Y. Nie, Y. Sheng, Q. Liu et al., "A regional-scale assessment of Himalayan glacial lake changes using satellite observations from 1990 to 2015," *Remote Sensing of Environment*, vol. 189, pp. 1–13, 2017.
- [34] Y. Zhang, G. Zhang, and T. Zhu, "Seasonal cycles of lakes on the Tibetan Plateau detected by Sentinel-1 SAR data," *Science of the Total Environment*, vol. 703, article 135563, 2020.
- [35] A. Sakai, T. Nuimura, K. Fujita, S. Takenaka, H. Nagai, and D. Lamsal, "Climate regime of Asian glaciers revealed by GAMDAM glacier inventory," *The Cryosphere*, vol. 9, no. 3, pp. 865–880, 2015.
- [36] H. Lu, M. Z. Liu, and X. Han, "The effects of forest litter on snow energy budget in the Tianshan Mountains, China," *Hydrological Processes*, vol. 31, no. 8, pp. 1602–1612, 2017.
- [37] M. N. Anjum, I. Ahmad, Y. Ding et al., "Assessment of IMERG-V06 precipitation product over different hydro-climatic regimes in the Tianshan Mountains, North-Western China," *North-Western China, Remote Sensing*, vol. 11, no. 19, p. 2314, 2019.
- [38] J. Fan, C. An, X. Zhang, X. Li, and J. Tan, "Hazard assessment of glacial lake outburst floods in Southeast Tibet based on RS and GIS technologies," *International Journal of Remote Sensing*, vol. 40, no. 13, pp. 4955–4979, 2019.
- [39] B. S. Krumwiede, U. Kamp, G. J. Leonard, J. S. Kargel, A. Dashtseren, and M. Walther, "Recent glacier changes in the Mongolian Altai Mountains: case studies from Munkh Khaikhan and Tavan Bogd," *Global Land Ice Measurements from Space*, 2014.
- [40] J. Li, T. A. Warner, Y. Wang, J. Bai, and A. Bao, "Mapping glacial lakes partially obscured by mountain shadows for time series and regional mapping applications," *International Journal of Remote Sensing*, vol. 40, no. 2, pp. 615–641, 2019.
- [41] J. Xiong, P. S. Thenkabail, M. K. Gumma et al., "Automated cropland mapping of continental Africa using Google Earth Engine cloud computing," *Isprs Journal of Photogrammetry & Remote Sensing*, vol. 126, pp. 225–244, 2017.
- [42] D. H. Shugar, A. Burr, U. K. Haritashya et al., "Rapid worldwide growth of glacial lakes since 1990," *Nature Climate Change*, vol. 10, pp. 939–945, 2020.
- [43] X. Zhang, L. Liu, X. Chen, Y. Gao, and M. Jiang, "Automatically monitoring impervious surfaces using spectral generalization and time series Landsat imagery from 1985 to 2020 in the Yangtze River Delta," *Journal of Remote Sensing*, vol. 2021, article 9873816, 16 pages, 2021.
- [44] A. Ashraf, R. Naz, and M. B. Iqbal, "Altitudinal dynamics of glacial lakes under changing climate in the Hindu Kush, Karakoram, and Himalaya ranges," *Geomorphology*, vol. 283, pp. 72–79, 2017.
- [45] X. Wang, Y. Ding, S. Liu et al., "Changes of glacial lakes and implications in Tian Shan, central Asia, based on remote sensing data from 1990 to 2010," *Environmental Research Letters*, vol. 8, no. 4, pp. 575–591, 2013.
- [46] F. Salerno, S. Thakuri, C. D'Agata et al., "Glacial lake distribution in the Mount Everest region: uncertainty of measurement and conditions of formation," *Global and Planetary Change*, vol. 92–93, pp. 30–39, 2012.
- [47] K. Gao, A. Duan, D. Chen, and G. Wu, "Surface energy budget diagnosis reveals possible mechanism for the different warming rate among Earth's three poles in recent decades," *Science Bulletin*, vol. 64, no. 16, pp. 1140–1143, 2019.
- [48] P. Shi, J. Zeng, K.-S. Chen, H. Ma, H. Bi, and C. Cui, "The 20-year spatiotemporal trends of remotely sensed soil moisture and vegetation and their response to climate change over the third pole," *Journal of Hydrometeorology*, vol. 22, pp. 2877–2896, 2021.
- [49] L. Huang, Z. Li, J. M. Zhou, and P. Zhang, "An automatic method for clean glacier and nonseasonal snow area change estimation in High Mountain Asia from 1990 to 2018,"

- Remote Sensing of Environment*, vol. 258, article 112376, 2021.
- [50] G. Zhang, T. Yao, W. Chen et al., "Regional differences of lake evolution across China during 1960s-2015 and its natural and anthropogenic causes," *Remote Sensing of Environment*, vol. 221, pp. 386–404, 2019.
- [51] G. Li and H. Lin, "Recent decadal glacier mass balances over the Western Nyainqentanglha Mountains and the increase in their melting contribution to Nam Co Lake measured by differential bistatic SAR interferometry," *Global and Planetary Change*, vol. 149, pp. 177–190, 2017.
- [52] J. Zhou, L. Wang, Y. Zhang, Y. Guo, X. Li, and W. Liu, "Exploring the water storage changes in the largest lake (Selin Co) over the Tibetan Plateau during 2003–2012 from a basin-wide hydrological modeling," *Water Resources Research*, vol. 51, no. 10, pp. 8060–8086, 2015.
- [53] C. Haemmig, M. Huss, H. Keusen et al., "Hazard assessment of glacial lake outburst floods from Kyagar Glacier, Karakoram Mountains, China," *Annals of Glaciology*, vol. 55, no. 66, pp. 34–44, 2014.
- [54] L. Huang, Z. Li, H. Han, B. Tian, and J. Zhou, "Analysis of thickness changes and the associated driving factors on a debris-covered glacier in the Tianshan Mountain," *Remote Sensing of Environment*, vol. 206, pp. 63–71, 2018.
- [55] D. E. Shean, S. Bhushan, P. Montesano, D. R. Rounce, A. Arendt, and B. Osmanoglu, "A systematic, regional assessment of high mountain Asia glacier mass balance," *Frontiers in Earth Science*, vol. 7, p. 363, 2020.
- [56] F. Brun, E. Berthier, P. Wagnon, A. Käab, and D. Treichler, "A spatially resolved estimate of High Mountain Asia glacier mass balances from 2000 to 2016," *Nature Geoscience*, vol. 10, no. 9, pp. 668–673, 2017.
- [57] J. Gardelle, E. Berthier, Y. Arnaud, and A. Käab, "Region-wide glacier mass balances over the Pamir-Karakoram-Himalaya during 1999–2011," *The Cryosphere*, vol. 7, no. 4, pp. 1263–1286, 2013.
- [58] A. Bhardwaj, P. K. Joshi, L. Snehmani et al., "Applicability of Landsat 8 data for characterizing glacier facies and supraglacial debris," *International Journal of Applied Earth Observation and Geoinformation*, vol. 38, pp. 51–64, 2015.
- [59] X. Wang, Q. Liu, S. Liu, J. Wei, and Z. Jiang, "Heterogeneity of glacial lake expansion and its contrasting signals with climate change in Tarim Basin, Central Asia," *Central Asia, Environmental earth sciences*, vol. 75, no. 8, 2016.
- [60] C. Song, Y. Sheng, L. Ke, Y. Nie, and J. Wang, "Glacial lake evolution in the southeastern Tibetan Plateau and the cause of rapid expansion of proglacial lakes linked to glacial-hydrogeomorphic processes," *Journal of Hydrology*, vol. 540, pp. 504–514, 2016.
- [61] X. Wang, K. Chai, S. Liu, J. Wei, Z. Jiang, and Q. Liu, "Changes of glaciers and glacial lakes implying corridor-barrier effects and climate change in the Hengduan Shan, southeastern Tibetan Plateau," *Journal of Glaciology*, vol. 63, no. 239, pp. 535–542, 2017.
- [62] T. Bolch, J. Peters, A. Yegorov, B. Pradhan, M. Buchroithner, and V. Blagoveshchensky, "Identification of potentially dangerous glacial lakes in the northern Tien Shan," *Natural Hazards*, vol. 59, no. 3, pp. 1691–1714, 2011.
- [63] A. Ashraf, M. B. Iqbal, N. Mustafa, R. Naz, and B. Ahmad, "Prevalent risk of glacial lake outburst flood hazard in the Hindu Kush–Karakoram–Himalaya region of Pakistan," *Environmental Earth Sciences*, vol. 80, no. 12, 2021.
- [64] S. Jiang, Y. Nie, Q. Liu et al., "Glacier change, supraglacial debris expansion and glacial lake evolution in the Gyirong River Basin, Central Himalayas, between 1988 and 2015," *Remote Sensing*, vol. 10, no. 7, p. 986, 2018.
- [65] A. M. Braga, R. C. Marques, F. A. Rodrigues, and F. N. Medeiros, "A median regularized level set for hierarchical segmentation of SAR images," *IEEE Geoscience and Remote Sensing Letters*, vol. 14, no. 7, pp. 1171–1175, 2017.
- [66] R. Jin, J. Yin, W. Zhou, and J. Yang, "Level set segmentation algorithm for high-resolution polarimetric SAR images based on a heterogeneous clutter model," *IEEE Journal of Selected Topics in Applied Earth Observations and Remote Sensing*, vol. 10, no. 10, pp. 4565–4579, 2017.
- [67] J. Wang, F. Chen, M. Zhang, and B. Yu, "NAU-net: a new deep learning framework in glacial Lake detection," *IEEE Geoscience and Remote Sensing Letters*, vol. 19, 2022.
- [68] Y. Yang, Z. Li, L. Huang, B. Tian, and Q. Chen, "Extraction of glacier outlines and water-eroded stripes using high-resolution SAR imagery," *International Journal of Remote Sensing*, vol. 37, no. 5, pp. 1016–1034, 2016.
- [69] Y. Sheng, C. Song, J. Wang et al., "Representative lake water extent mapping at continental scales using multi-temporal Landsat-8 imagery," *Remote Sensing of Environment*, vol. 185, pp. 129–141, 2016.
- [70] A. Sakai, "Brief communication: updated GAMDAM glacier inventory over high-mountain Asia," *The Cryosphere*, vol. 13, no. 7, pp. 2043–2049, 2019.
- [71] D. Scherler, H. Wulf, and N. Gorelick, "Global assessment of supraglacial debris-cover extents," *Geophysical Research Letters*, vol. 45, no. 21, pp. 11,798–11,805, 2018.
- [72] Z. Zhu and C. E. Woodcock, "Object-based cloud and cloud shadow detection in Landsat imagery," *Remote Sensing of Environment*, vol. 118, pp. 83–94, 2012.